nature communications

Article

https://doi.org/10.1038/s41467-025-57517-y

Elevated NAD$^+$ drives Sir2A-mediated GCβ deacetylation and OES localization for Plasmodium ookinete gliding and mosquito infection

Received: 3 October 2024

Accepted: 25 February 2025

Published online: 06 March 2025

Check for updates

Yang Shi[1], Lin Wan[1], Mengmeng Jiao[1], Chuan-qi Zhong[1] ✉, Huiting Cui[1] ✉ & Jing Yuan[1,2] ✉

cGMP signal-activated ookinete gliding is essential for mosquito midgut infection of *Plasmodium* in malaria transmission. During ookinete development, cGMP synthesizer GCβ polarizes to a unique localization "ookinete extrados site" (OES) until ookinete maturation and activates cGMP signaling for initiating parasite motility. However, the mechanism underlying GCβ translocation from cytosol to OES remains elusive. Here, we use protein proximity labeling to search the GCβ-interacting proteins in ookinetes of the rodent malaria parasite *P. yoelii*, and find the top hit Sir2A, a NAD$^+$-dependent sirtuin family deacetylase. Sir2A interacts with GCβ throughout ookinete development. In mature ookinetes, Sir2A co-localizes with GCβ at OES in a mutually dependent manner. Parasites lacking Sir2A lose GCβ localization at OES, ookinete gliding, and mosquito infection, phenocopying GCβ deficiency. GCβ is acetylated at gametocytes but is deacetylated by Sir2A for OES localization at mature ookinetes. We further demonstrate that the level of NAD$^+$, an essential co-substrate for sirtuin, increases during the ookinete development. NAD$^+$ at its maximal level in mature ookinetes promotes Sir2A-catalyzed GCβ deacetylation, ensuring GCβ localization at OES. This study highlights the spatiotemporal coordination of cytosolic NAD$^+$ level and NAD$^+$-dependent Sir2A in regulating GCβ deacetylation and dynamic localization for *Plasmodium* ookinete gliding.

Malaria, caused by the protozoan parasite *Plasmodium*, is an infectious disease resulting in an estimated 49 million cases and 608,000 deaths globally in 2022[1]. The spread of malaria relies on parasite infection and development in the mosquito vector. Once entering the mosquito midgut after a blood meal, male and female gametocytes are immediately activated and develop into male and female gametes, which fertilize to form the zygotes. Within 12 to 20 h, the spherical zygotes undergo remarkable morphogenesis of "protrusion-elongation-maturation" to differentiate into crescent-shaped ookinetes[2,3]. Only mature ookinetes activating gliding motility could move through the blood bolus and traverse the midgut epithelium barrier. Following colonization at the midgut basal lamina, the ookinete develops into an oocyst, each giving rise to thousands of sporozoites[4,5]. When

[1]State Key Laboratory of Cellular Stress Biology, School of Life Sciences, Faculty of Medicine and Life Sciences, Xiamen University, Xiamen, China. [2]Department of Infectious Disease, Xiang'an Hospital of Xiamen University, School of Medicine, Faculty of Medicine and Life Sciences, Xiamen University, Xiamen, China. ✉e-mail: zhongcq@xmu.edu.cn; cuihuiting@xmu.edu.cn; yuanjing@xmu.edu.cn

mosquitoes bite again, the sporozoites in the salivary glands are injected into another vertebrate host.

Ookinete motility is powered by the glideosome, an actomyosin-based protein machinery located between the parasite plasma membrane (PPM) and the underneath membranal organelle of the inner membrane complex (IMC)[6,7]. The mechanical force produced by the glideosome is converted to the backward movement of the adhesin protein CTRP[8], generating parasite forward movement for gliding or invasion[9]. 3′-5′-cyclic guanosine monophosphate (cGMP), guanylate cyclase beta (GCβ), phosphodiesterase delta (PDEδ), and cGMP-dependent protein kinase G (PKG) play critical roles in upstream signaling of ookinete motility. In mature ookinete, the gliding initiation depends on the activation of cGMP signal[10–12], which level is coordinated by the activities of GCβ (synthesizes cGMP) and PDEδ (hydrolyzes cGMP)[12]. Only the cGMP level exceeding the threshold could activate PKG, resulting in PLC/IP3-mediated Ca^{2+} release, phosphorylation of multiple glideosome proteins, and initiation of ookinete gliding[11–13].

Plasmodium parasites encode two guanylyl cyclases GCα and GCβ[14–16]. Both GCs are large proteins (3000–4000 amino acids in length) possessing an unusual protein architecture, in which the C-terminal guanylate cyclase domain (GCD) is combined with an unrelated N-terminal P4-type ATPase-like domain (ALD)[17,18]. While the GCD is responsible for cGMP synthesis, the function of the ALD is still obscure[14–16]. GCβ is genetically essential for ookinete gliding in *P. berghei*, *P. yoelii*, and *P. falciparum*[10–12,19]. Due to the large size, multiple transmembrane helixes, and the ALD-GCD hybrid domain structure of GCβ, the geography of GCβ-mediated cGMP signaling in the *Plasmodium* ookinete gliding remained elusive for a long time[20–22].

As our previous efforts to investigate the expression and localization of GCβ and PDEδ in ookinete gliding, we revealed a spatiotemporal regulation of the cGMP signal in the *P. yoelii*[19]. During the ookinete development, GCβ and PDEδ are distributed in the cytoplasm. Until ookinete maturation, GCβ translocates and polarizes to PPM at the "ookinete extrados site" (OES) while PDEδ maintains cytosolic[19]. The OES is a subapical area in the outer curve of the crescent ookinete[19,21,22]. GCβ polarization at OES initiates the gliding of mature ookinete. In addition, the P4-ATPase co-factor CDC50A is also localized at OES and functions as a chaperone to stabilize GCβ[19]. Based on these results, we proposed a GCβ/CDC50A polarization-directed cGMP signal activation model for ookinete gliding[19]. Before ookinete maturation, GCβ/CDC50A complex and PDEδ maintain a subthreshold cGMP level precluding PKG activation in the cytoplasm. Upon ookinete maturation, GCβ/CDC50A complex translocates to OES. The GCβ/CDC50A polarization increases the local cGMP concentration that drives PKG activation and initiates ookinetes gliding[19]. Despite the progress in understanding cGMP signaling of ookinete gliding, the mechanism underlying GCβ translocation from cytosol to OES until mature ookinete remains unknown.

Protein acetylation is a posttranslational modification regulating protein stability, localization, and protein-protein interaction[23,24]. Protein acetylation is dynamically controlled by acetylase and deacetylase[24,25]. The silent information regulator 2 family proteins of deacetylase (Sirtuin or SIRT) are found in organisms ranging from bacteria to humans[26]. Sirtuins deacetylate the acetyl-lysine residue from the acetylated substrates and its catalytic activity depends on the level of the nicotinamide adenine dinucleotide (NAD^+)[27,28]. *Plasmodium* parasites encode two sirtuin proteins Sir2A and Sir2B[29]. The *P. falciparum* parasite evolves the antigenic variation at the infected erythrocyte surface to avoid host immune clearance via regulated gene expression of the *var* gene family-encoded antigens[30,31]. In the asexual blood stages of *P. falciparum*, Sir2A is thought to regulate histone deacetylation in the telomeric regions and control the antigenic expression of the *var* genes[30]. So far, the role of Sir2A has not been investigated in the mosquito stages of *Plasmodium*.

In this work, we search the GCβ-interacting proteins at OES in the *P. yoelii* ookinetes and find that Sir2A forms a complex with GCβ/CDC50A during ookinete development. Parasites lacking Sir2A phenocopy GCβ deficiency in ookinete gliding. Sir2A catalyzes GCβ deacetylation and modulates GCβ localization at OES in mature ookinete. We further demonstrate that the level of NAD^+, an essential co-substrate of Sir2A, increases during the ookinete development. The NAD^+ at its maximal level promotes Sir2A-catalyzed GCβ deacetylation until ookinete maturation.

Results

Proximity proteomics identifies Sir2A a potential GCβ-interacting protein in ookinete of *P. yoelii*

To search potential regulators of GCβ localization at OES, we applied the biotin ligase TurboID-based proximity labeling (PL) to track the GCβ-interacting proteins in the ookinetes. The endogenous GCβ was fused with a TurboID::6HA domain via CRISPR-Cas9 in the *P. yoelii* 17XNL strain, generating the modified line *gcβ::TurboID* (*Tb-GCβ* in short) (Fig. 1A). We generated a control line *gcβ::T2A::TurboID::6HA* (*Tb-Cyto* in short), in which a "ribosome skip" T2A peptide (EGRGSLLTCGDVEENPGP) was inserted between GCβ and TurboID::6HA to direct cytosolic expression of TurboID::6HA alone under the promoter of *gcβ* gene (Fig. 1A). As expected, the fusion protein Tb-GCβ was localized at OES while the Tb-Cyto was cytosolic in the ookinetes (Fig. 1A). After incubation with 50 μM biotin for 3 h at 22 °C, the ookinetes expressing ligase were co-stained with fluorescence-conjugated streptavidin and anti-HA antibody. As expected, the biotinylated proteins were co-localized with the fusion ligase at OES in the *Tb-GCβ* ookinetes, while the biotinylated proteins and the ligase were in cytosolic in *Tb-Cyto* ookinetes (Fig. 1A). Three biological replicates were prepared from the *Tb-GCβ* and *Tb-Cyto* ookinetes, and the streptavidin-affinity purified proteins from cell extracts were subjected to proteomic analysis. Quantitative mass spectrometry yielded 251 enriched proteins with high confidence in *Tb-GCβ* compared to *Tb-Cyto* ookinetes (Fig. 1B and Supplementary Data 1). GCβ, after being cis-biotinylated, was included in these protein hits (blue dot in Fig. 1B). CDC50A, an essential cofactor of GCβ[19], was also detected (blue dot in Fig. 1B), indicating the good quality of these PL experiments. Among the significant hits, the top is the sirtuin family protein Sir2A (red dot in Fig. 1B). So far, the expression, localization, and function of Sir2A have not been investigated in mosquito stages of *Plasmodium*, including the ookinete.

To validate the PL results and investigate the expression and localization of Sir2A during the parasite life cycle of *P. yoelii*, we tagged the endogenous Sir2A (PY17X_1348600) with a sextuple HA epitope (6HA) at C-terminus in the 17XNL strain using CRISPR/Cas9[32,33]. The tagged parasite line *sir2a::6HA* developed normally in mice and mosquitoes, indicating no detectable detrimental effect of tagging on protein function. Immunoblot and immunofluorescence assay (IFA) showed that Sir2A was expressed in gametocytes, ookinetes, mosquito midgut oocysts, and mosquito salivary gland sporozoites, but was not detected in asexual blood stage parasites (Fig. 1C and D). Co-staining of the *sir2a::6HA* gametocytes with α-TubulinII (male gametocyte highly expressed) and HA antibodies showed that Sir2A was expressed only in female gametocytes (Fig. 1E). Interestingly, Sir2A was distributed in the cytoplasm of gametocytes, oocysts, and sporozoites, but was concentrated at a site posterior to the apical of ookinetes (Fig. 1D). This area in ookinetes was designated as the "ookinete extrados site" (OES)[19]. During the in vitro zygote to ookinete differentiation, Sir2A was distributed in the cytoplasm from zygote to retort, but concentrated to OES in mature ookinetes (Fig. 1F). We quantified the polarization level of Sir2A by calculating fluorescent signals at OES over the whole cell at different stages of ookinete development (Fig. 1G). We generated another parasite line *sir2a::3V5* in which the endogenous Sir2A was tagged with a triple V5 epitope (3V5) in the

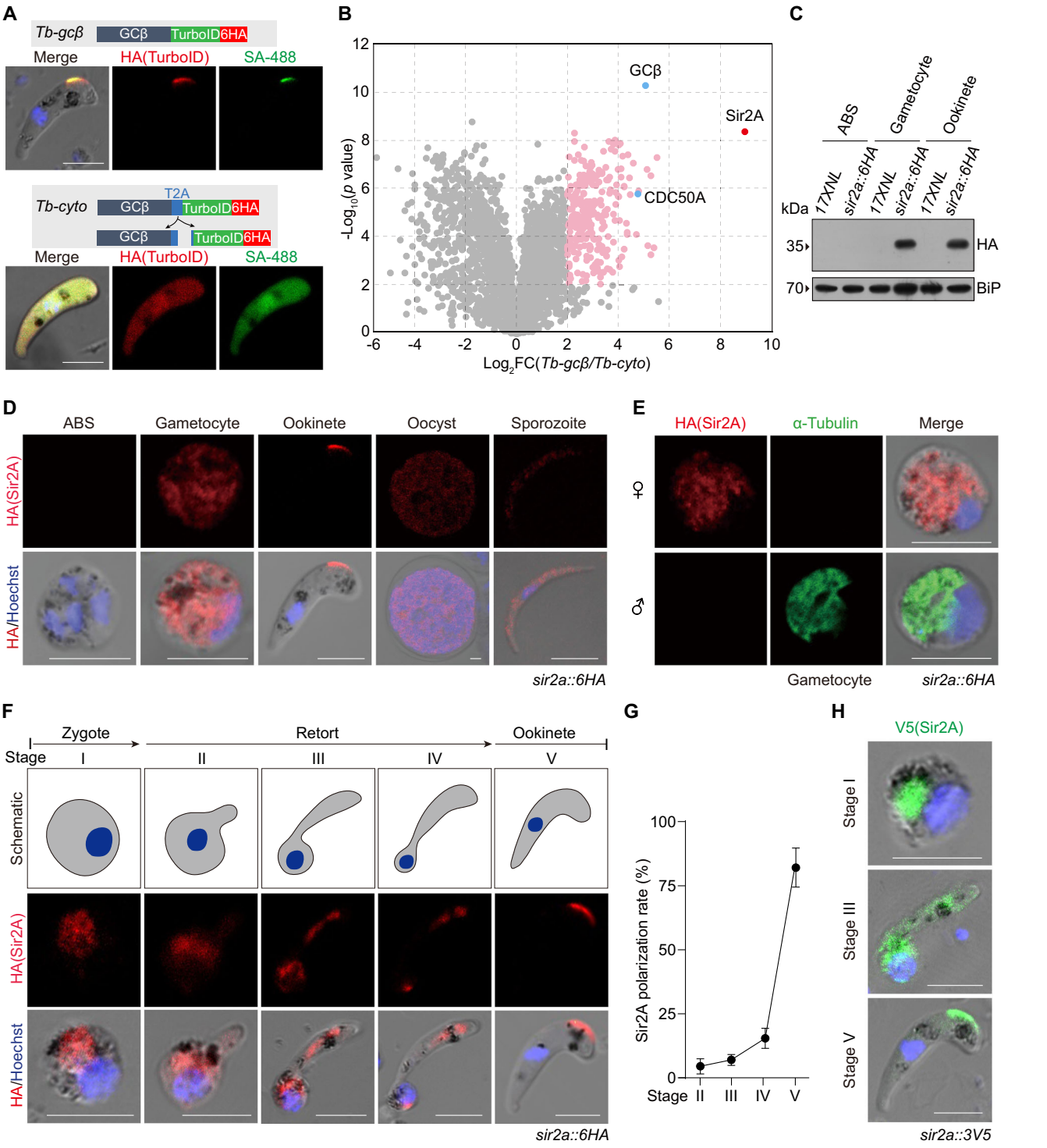

C-terminus and observed similar expression and localization of Sir2A during zygote to ookinete differentiation (Fig. 1H). Together, we identified Sir2A as a potential GCβ-interacting protein at OES in the ookinetes. Sir2A had a dynamical localization pattern during zygote to ookinete development, similar to the GCβ/CDC50A complex[19].

Sir2A co-localizes and interacts with GCβ/CDC50A during ookinete development

We investigated the temporal-spatial association between Sir2A and GCβ during the gametocyte-zygote-ookinete development. From the parasite *gcβ::6HA* generated previously[19], the endogenous Sir2A was tagged with a 3V5 at the C-terminus, generating a double-tagged line *gcβ::6HA;sir2a::3V5*. In this line, we analyzed the time-course localization dynamic of Sir2A and GCβ. In the female gametocytes, Sir2A and GCβ were cytosolic but not overlaid with each other (Fig. 2A). After gamete fertilization, Sir2A became co-localized with GCβ at the cytosol in the zygotes until later-stage retorts. In mature ookinetes, both Sir2A and GCβ were concentrated to OES (Fig. 2A). We used different methods to analyze the association between Sir2A and GCβ during gametocyte-zygote-ookinete development. Co-immunoprecipitation (Co-IP) also revealed that Sir2A did not interact with GCβ in gametocytes of the *gcβ::6HA;sir2a::3V5* (*DTS1*) parasites (Fig. 2B). As a positive control, GCβ bound its cofactor CDC50A in gametocytes of the *gcβ::6HA;50a::3V5* (*DTS2*) parasites[19] (Fig. 2B). Proximity Ligation Assay

Fig. 1 | Proximity proteomics identifies Sir2A a potential GCβ-interacting protein in ookinete of *P. yoelii*. **A** Schematic of the modified line used for TurboID ligase-mediated proximity labeling of GCβ-interacting proteins in living ookinetes. Endogenous GCβ was C-terminally tagged with a TurboID::6HA motif by CRISPR-Cas9 in 17XNL, generating *Tb-gcβ* line. *Tb-Cyto* is a control line in which the T2A is inserted between GCβ and TurboID for separated expression of GCβ and TurboID. Co-staining of HA-tagged TurboID ligase (red) and biotinylated proteins (SA-488, green) in ookinetes after incubation with 50 μM biotin at 22 °C for 3 h. Scale bars: 5 μm. A representative for three independent experiments. **B** Volcano plots showing 251 significantly enriched proteins (cutoffs $\log_2$FC ≥ 1 and *p*-value ≤ 0.05) in *Tb-gcβ* versus *Tb-Cyto* ookinetes. The protein list is in Supplementary Data 1. The protein's relative enrichment ratio (*x*-axis) was calculated by quantifying protein intensity in *Tb-gcβ* relative to *Tb-Cyto* ($n = 3$). The *p*-values were calculated by a two-sided *t* test. GCβ, CDC50A, and Sir2A are highlighted. **C** Immunoblot of Sir2A in asexual blood stages (ABS), gametocytes, and ookinetes of 17XNL and *sir2a::6HA* parasites. BiP was used as a loading control. A representative for three independent experiments. **D** Immunofluorescence assay (IFA) detecting Sir2A expression in multiple stages of the *sir2a::6HA* parasite. The parasites were co-stained with anti-HA antibody and DNA dye Hoechst 33342. Scale bar: 5 μm. A representative for three independent experiments. **E** Co-staining *sir2a::6HA* gametocytes with antibodies against HA and α-Tubulin II (male gametocyte-specific protein). Scale bar: 5 μm. A representative for three independent experiments. **F** IFA of Sir2A expression dynamics during the zygote to ookinete development of *sir2a::6HA* parasite. Scale bars: 5 μm. A representative for three independent experiments. **G** Quantification of Sir2A polarization level at OES during the in vitro ookinete development in (**F**). Polarization rates are mean ± SD of three independent experiments. Thirty ookinetes were analyzed for each group in each experiment. **H** IFA of Sir2A expression dynamics during the zygote to ookinete development of *sir2a::3V5* parasite. Scale bars: 5 μm. Representative for three independent experiments.

(PLA) is an immunohistochemical tool to detect protein interaction with specificity and sensitivity[34]. As a positive control, PLA signals indicating GCβ and CDC50A interaction were detected in the *gcβ::6HA;50a::3V5* gametocytes (Fig. 2C). No PLA signal was detected in the *gcβ::6HA;sir2a::3V5* gametocytes when using both anti-HA and anti-V5 antibodies (Fig. 2C). In contrast, both Co-IP and PLA detected that Sir2A co-localized and interacted with GCβ at cytosol in the zygotes (Fig. 2D and E) and at OES in the ookinetes (Fig. 2F and G).

Since CDC50A is a cofactor of GCβ[19], we also analyzed the association between Sir2A and CDC50A in this development. From the previous parasite line *cdc50a::6HA*[19], we tagged the endogenous Sir2A with a 3V5 and obtained another double-tagged line *cdc50a::6HA;-sir2a::3V5* (*DTS3*). Sir2A co-localized and interacted with CDC50A in zygotes and ookinetes in both IFA and Co-IP (Fig. 2H and I), showing a similar association pattern as with GCβ. These results demonstrated that Sir2A does not interact with GCβ/CDC50A in the gametocytes but forms a complex with GCβ/CDC50A during the zygote to ookinete development.

Sir2A phenocopies GCβ in regulating ookinete gliding for mosquito midgut infection

The *P. yoelii* Sir2A (PY17X_1348600) is a 278 amino acid protein that shows high identity to Sir2A proteins from the rodent malaria parasite *P. berghei* and human malaria parasites *P. falciparum* and *P. vivax* (Supplementary fig. 1). To elucidate the function of Sir2A in the ookinetes, we deleted the whole coding region (837 bp) of the *sir2a* gene by homologous recombination via CRISPR-Cas9 in the *P. yoelii* 17XNL strain (wild-type) and obtained a mutant clone Δ*sir2a* (Fig. 3A). The Δ*sir2a* exhibited normal asexual blood stage proliferation and gametocyte formation in the mice (Fig. 3B and C). To evaluate the role of Sir2A in parasite development in the mosquito, *Anopheles stephensi* mosquitoes were fed on the parasite-infected mice. Δ*sir2a* produced no oocyst in the midgut on day 7 post-infection (pi) (Fig. 3D) and no sporozoites in the salivary glands on day 14 pi (Fig. 3E), indicating parasite transmission failure in the mosquito. As a parallel test, the GCβ-null parasite Δ*gcβ* failed to develop both oocyst and sporozoite in the mosquitoes as expected[12] (Fig. 3D and E).

The *Plasmodium* undergoes a gametocyte-gamete-zygote-ookinete development in the mosquito midgut and forms the crescent-shaped motile ookinetes for penetration. We performed experiments to delineate the steps affected by Sir2A deficiency. The Δ*sir2a* showed normal male and female gamete formation in vitro compared with 17XNL (Supplementary Fig. 2A and B). The in vitro assay for zygote to ookinete differentiation revealed that *sir2a* deletion had no marked effect on ookinete formation (Fig. 3F). We isolated the Δ*sir2a* parasites from infected mosquito midguts and observed normal ookinetes (Fig. 3G). Under scanning electron microscopy, the Δ*sir2a* mature ookinetes displayed a typical crescent shape as 17XNL (Fig. 3H), suggesting no defect in the parasite morphology after loss of Sir2A. Since gliding motility is a prerequisite for the midgut traversal of ookinetes, we assessed the gliding capability of ookinetes using an in vitro Matrigel-based assay[11,35]. The Δ*sir2a* ookinetes displayed significantly reduced gliding speed compared to 17XNL but were slightly faster than the Δ*gcβ* ookinetes (17XNL: 7.9 ± 1.6 μm/min, $n = 25$; Δ*sir2a*: 1.4 ± 0.8 μm/min, $n = 28$; and Δ*gcβ*: 0.4 ± 0.4 μm/min, $n = 25$) (Fig. 3I). The gliding-deficient ookinete of Δ*sir2a* may fail to traverse mosquito midgut. To test it, the midguts from infected mosquitoes were dissected at 24 h pi (hpi) and visualized after staining with an antibody against P28 (a plasma membrane protein of ookinetes and early oocysts) (Fig. 3J). Reduced numbers of $P28^+$ parasites were detected in the midguts infected with Δ*sir2a* compared with 17XNL (midgut-associated parasites per mosquito: 91 ± 45 in 17XNL, $n = 30$; 3 ± 4 in Δ*sir2a*, $n = 35$; 0 ± 0 in Δ*gcβ*, $n = 29$) (Fig. 3K).

To confirm that the ookinete gliding defect was caused by Sir2A deletion, we re-introduced the deleted 837 bp part fused with a 3V5 back into the *sir2a* locus of the Δ*sir2a* parasite (Fig. 3A). Expression of the V5-tagged Sir2A was detected in gametocytes and ookinetes of the complemented line *Comp* (Fig. 3L). In line with the endogenous Sir2A, the 3V5::Sir2A fusion protein exhibited OES localization in the *Comp* ookinetes (Fig. 3L). Notably, the *Comp* parasite restored the oocyst and sporozoite formation in the infected mosquitoes (Fig. 3M and N). Furthermore, we generated another Sir2A null parasite line by deleting the *sir2a* gene in the *sir2a::6HA* parasite (Supplementary fig. 2C and D). Consistent with the phenotypes for the Δ*sir2a* parasites, the mutant parasite *sir2a::6HA*;Δ*sir2a* displayed similar defects in the ookinete gliding and mosquito transmission of the parasite (Supplementary fig. 2E to K). These results demonstrated that Sir2A regulates ookinete gliding (Fig. 3O), similar to the GCβ/CDC50A complex[19].

Mutual dependent localization of Sir2A and GCβ at OES in mature ookinete

We investigated whether Sir2A regulates GCβ expression or localization. The *sir2a* gene was deleted in the *gcβ::6HA* parasite, generating the mutant line *gcβ::6HA*;Δ*sir2a*. Immunoblot showed that Sir2A depletion did not affect protein levels of GCβ in gametocytes, zygotes, and ookinetes (Fig. 4A), ruling out an effect of Sir2A on GCβ protein synthesis or stability. IFA found that Sir2A depletion did not affect the cytosolic distribution of GCβ in gametocytes and zygotes, but GCβ lost polarization at OES and was distributed at cytosol in the *gcβ::6HA*;Δ*sir2a* ookinetes (Fig. 4B and C and Supplementary Fig. 3). To further validate the localization alteration of GCβ in ookinetes after loss of Sir2A, we isolated the heavy fraction (including pellicle membrane and cytoskeleton) and light fraction (including cytoplasm) from the extracts of ookinete after hypotonic lysis. Immunoblot detected GCβ in heavy fraction from the *gcβ::6HA* ookinetes, but mainly in light fraction from the *gcβ::6HA*;Δ*sir2a* ookinetes (Fig. 4D). These results in both IFA and protein fraction assays indicate that Sir2A is critical for GCβ localization at OES in ookinete.

https://doi.org/10.1038/s41467-025-57517-y

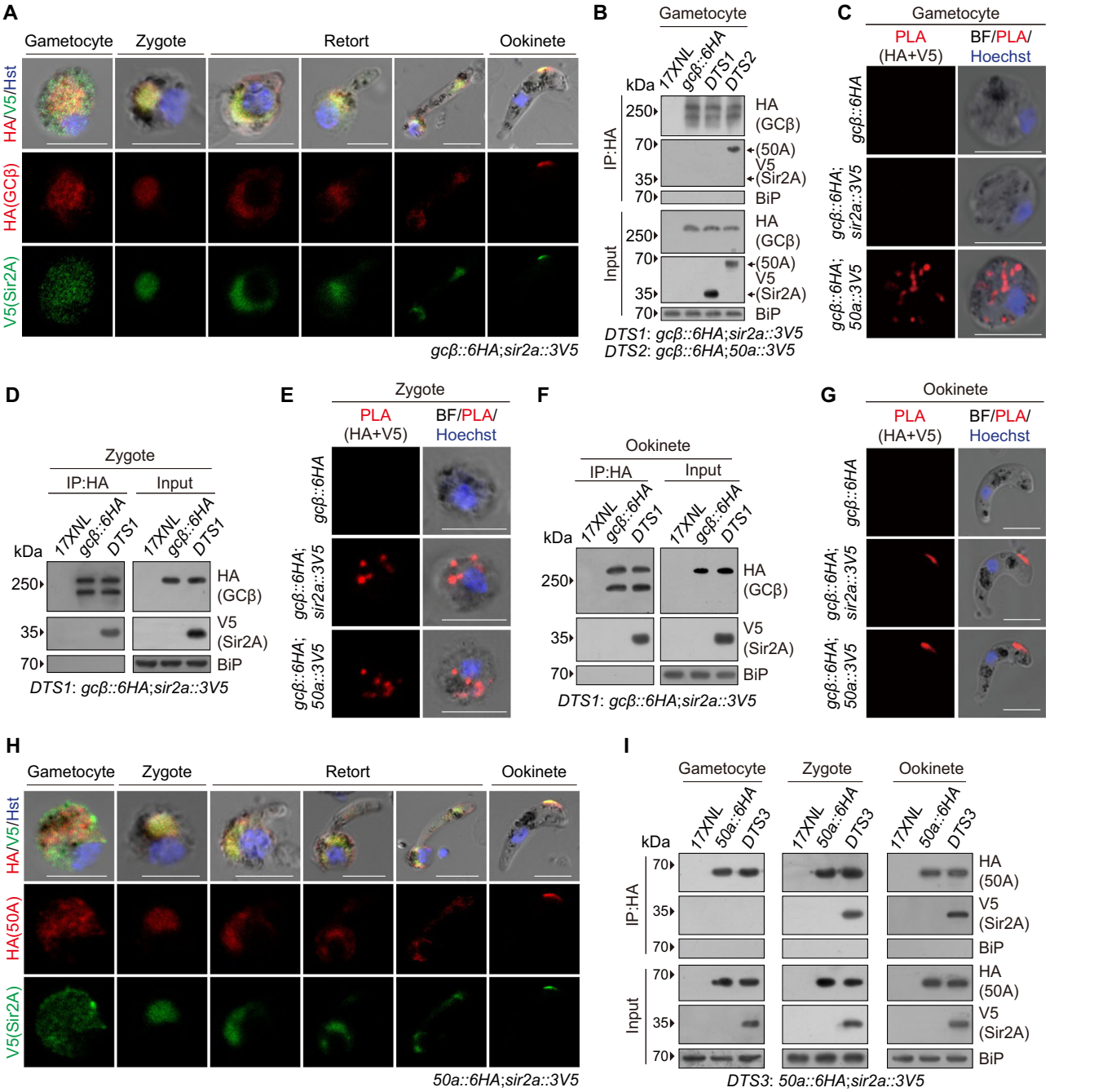

Fig. 2 | Sir2A co-localizes and interacts with GCβ/CDC50A during ookinete development. A IFA of HA-tagged GCβ and V5-tagged Sir2A expression during the gametocyte to ookinete development of the *gcβ::6HA;sir2a::3V5* parasite. Scale bars: 5 µm. A representative for three independent experiments. **B** Co-immunoprecipitation (Co-IP) of GCβ and Sir2A in gametocytes of the *gcβ::6HA;-sir2a::3V5* (*DTS1*) parasite. Co-IP was conducted using an anti-HA antibody. BiP as a loading control. Interaction between GCβ and CDC50A in *gcβ::6HA;cdc50a::3V5* (*DTS2*) gametocytes was used as a positive control. A representative for two independent experiments. **C** Proximity ligation assay (PLA) detecting protein interaction between GCβ and Sir2A in the *gcβ::6HA;sir2a::3V5* gametocytes. GCβ and CDC50A interaction in *gcβ::6HA;cdc50a::3V5* gametocytes was used as a positive control. Scale bars: 5 µm. A representative for two independent experiments. **D** Co-IP of GCβ and Sir2A in the *DTS1* zygotes. Co-IP was conducted using an anti-HA antibody. BiP as a loading control. A representative for two independent experiments. **E** PLA detecting protein interaction between GCβ and Sir2A in the *DTS1* zygotes. Scale bars: 5 µm. A representative for two independent experiments. **F** Co-IP of GCβ and Sir2A in the *DTS1* ookinetes. Co-IP was conducted using an anti-HA antibody. BiP as a loading control. A representative for two independent experiments. **G** PLA detecting protein interaction between GCβ and Sir2A in the *DTS1* ookinetes. Two independently performed experiments with similar results. Scale bars: 5 µm. **H** IFA of HA-tagged CDC50A and V5-tagged Sir2A expression during the gametocyte to ookinete development of the *50a::6HA;sir2a::3V5* parasite. Scale bars: 5 µm. A representative for three independent experiments. **I** Co-IP of CDC50A and Sir2A in gametocyte, zygote, and ookinete of the *cdc50a::6HA;sir2a::3V5* (*DTS3*) parasite. Co-IP was conducted using an anti-HA antibody. BiP as a loading control. A representative for two independent experiments.

We next investigated whether GCβ, in turn, influences the Sir2A localization at OES in ookinete. We deleted the *gcβ* gene in the *sir2a::6HA* parasite and obtained the mutant clone *sir2a::6HA;Δgcβ*. Deleting *gcβ* had no impact on Sir2A protein abundance in gametocytes, zygotes, and ookinetes (Fig. 4E). Interestingly, GCβ depletion did not affect the cytosolic distribution of Sir2A in gametocytes and zygotes, but Sir2A lost polarization at OES and was distributed at cytosol in the *sir2a::6HA;Δgcβ* ookinetes (Fig. 4F and G).

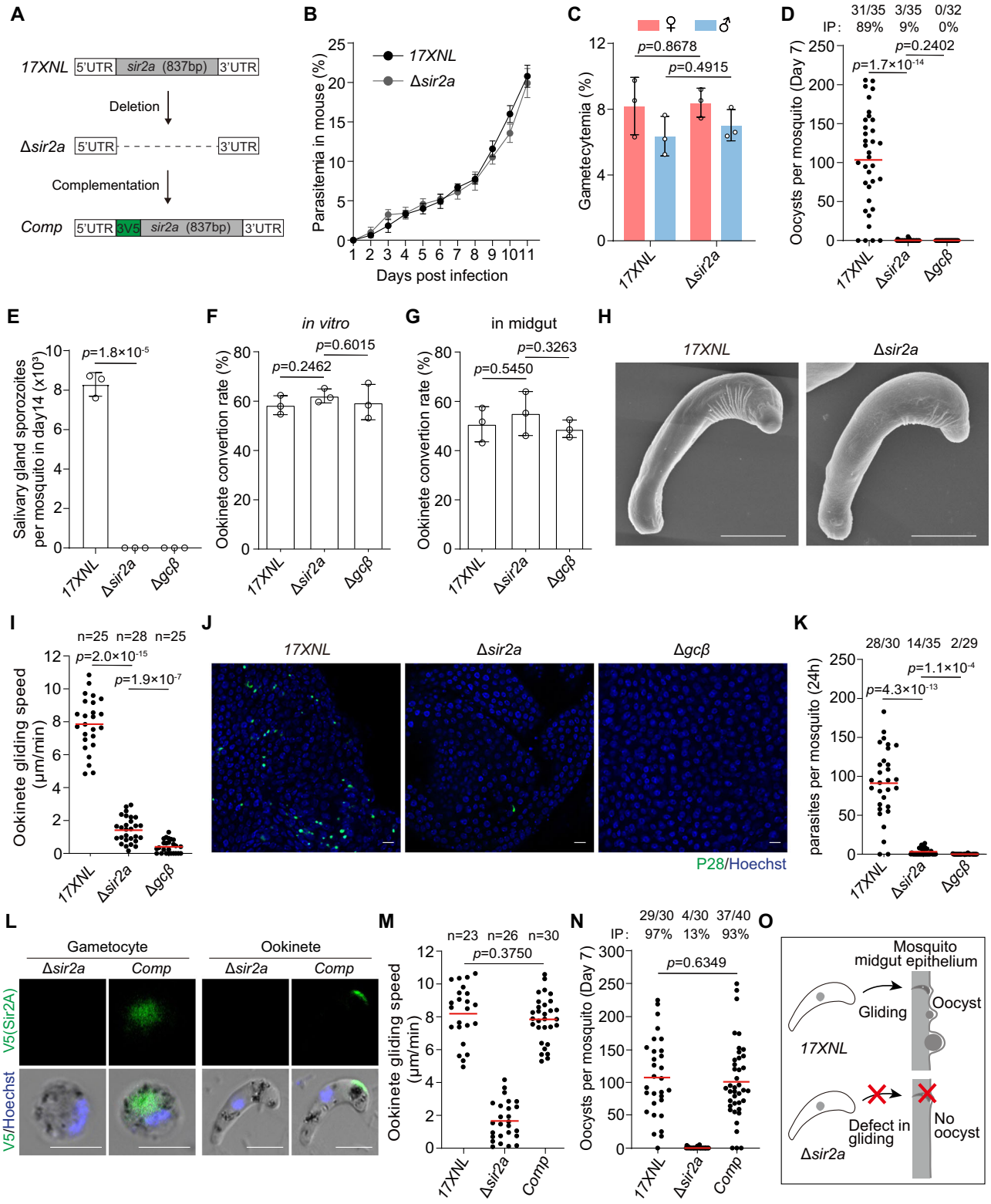

Therefore, Sir2A and GCβ are localized at OES in ookinetes in a mutually dependent manner (Fig. 4H).

We additionally analyzed the effect of Sir2A depletion on the protein expression and localization of PDEδ (cGMP-degrading enzyme) and PKG (direct effector of cGMP). The *sir2a* gene was deleted in two parasite lines *pdeδ::4Myc* and *pkg::4Myc*[19], and we obtained two mutant lines *pdeδ::4Myc;Δsir2a* and *pkg::4Myc;Δsir2a*. Deleting *sir2a* had no impact on protein abundance and localization of PDEδ and PKG in ookinetes (Supplementary fig. 4).

GCβ is acetylated at gametocytes and deacetylated at mature ookinetes

Since Sir2A is a putative deacetylase, we suspected GCβ as a substrate of Sir2A. We tested whether GCβ/CDC50A is acetylated in gametocytes and deacetylated in ookinetes. Immunoblot of the HA antibody-immunoprecipitated GCβ from *gcβ::6HA* gametocyte extracts detected acetylation signals for GCβ::6HA using the pan-acetylation antibody Ac-K (Fig. 5A). We generated another parasite line *gcβ::3V5* in which the endogenous GCβ was C-terminally tagged with a 3V5 and

Fig. 3 | Sir2A phenocopies GCβ in regulating ookinete gliding for mosquito midgut infection. A Schematic of the *sir2a* gene deletion and complementation using CRISPR-Cas9. The whole coding region of *sir2a* was removed in the 17XNL parasite, generating the Δ*sir2a* mutant. The *sir2a* gene from *P. yoelii* fused with a 3V5 was introduced back to the *sir2a* locus of the Δ*sir2a* mutant, generating complemented line *Comp*. **B** Parasite proliferation at asexual blood stages in mice. Mean ± SD from three mice in each group. A representative for two independent experiments. **C** Male and female gametocyte formation in mice. Mean ± SD from three mice in each group, two-tailed *t* test. A representative for two independent experiments. **D** Midgut oocyst formation in mosquitos at day 7 post-infection. x/y on the top is the number of mosquitoes containing oocyst/the number of dissected mosquitoes, and the percentage represents the infection prevalence of mosquitoes. The red lines show the mean value. Two-sided Mann-Whitney *U* test. A representative for two independent experiments. **E** Salivary gland sporozoite formation in mosquitoes at day 14 post-infection. Thirty infected mosquitoes were counted in each group. Mean ± SD from three independent experiments, two-tailed *t* test. **F** Mature ookinete formation in vitro. Mean ± SD from three independent experiments, two-tailed *t* test. **G** Mature ookinete formation in the mosquito midgut. Mean ± SD from three independent experiments, two-tailed *t* test. **H** Scanning electron microscopy (SEM) of 17XNL and Δ*sir2a* ookinetes. Scale bars: 5 μm. A representative for three independent experiments. **I** Ookinete gliding motility using the in vitro Matrigel-based assay. n is the number of ookinetes analyzed. The red lines show the mean value. Two-sided Mann-Whitney *U* test. Representative for three independent experiments. **J** IFA of P28 in ookinete and early oocyst at mosquito midguts infected with 17XNL, Δ*sir2a*, and Δ*gcβ* parasites 24 h post-infection. P28 is a plasma membrane protein of ookinete and early oocyst. Scale bars: 20 μm. Representative for three independent experiments. **K** Quantification of parasites in (**J**). x/y on the top is the number of midguts containing parasite/the number of midguts measured, red lines show the mean value. Two-sided Mann-Whitney test. **L** IFA of the V5-tagged Sir2A in gametocytes and ookinetes of the complemented line *Comp*. Scale bar: 5 μm. Representative for three independent experiments. **M** Ookinete gliding motility. n is the number of ookinetes analyzed. The red lines show the mean value. Two-sided Mann-Whitney *U* test. Representative for three independent experiments. **N** Midgut oocyst formation in mosquitoes at day 7 post-infection. Red horizontal lines show the mean value, two-sided Mann-Whitney *U* test. x/y on the top is the number of mosquitoes containing oocyst/the number of mosquitoes dissected. The percentage represents the infection prevalence of mosquitoes. Representative for two independent experiments. **O** Cartoon showing Sir2A deficiency in ookinete gliding for mosquito midgut invasion.

also detected the acetylation signals for GCβ::3V5 from gametocyte extracts (Fig. 5B). In the parallel experiments, we analyzed the acetylation state of CDC50A and detected no acetylation signal for CDC50A::6HA from the *50a::6HA* gametocyte (Fig. 5C). These results demonstrated the acetylation in GCβ but not in CDC50A in gametocytes. Furthermore, we investigated the GCβ acetylation dynamic during the gametocyte-zygote-ookinete development of the *gcβ::6HA* parasite. The acetylation signal was detected for GCβ::6HA in gametocytes and zygotes but significantly decreased in ookinetes (Fig. 5D). These results indicated that GCβ is acetylated in gametocytes and zygotes but is deacetylated in mature ookinetes.

The *P. yoelii* GCβ is a 3,015 aa protein that contains 22 transmembrane helixes spanning an N-terminal ALD (1-1248 aa) and a C-terminal GCD (1249-3015 aa)[19] (Fig. 5E). Bioinformatics predicted 59 potential residues for acetylation in GCβ using the software GPS-Palm 4.0 (https://pail.biocuckoo.org/)[36]. We attempted to map the acetylated residues in GCβ using mass spectrometry but failed to collect enough endogenous protein. Alternatively, we characterized the acetylated domain of either ALD and (or) GCD in GCβ. We used a previously generated parasite line *gcβ::T2A*[19], in which a "ribosome skip" T2A peptide was introduced into the linker region between ALD and GCD in the *gcβ::6HA* parasite (Fig. 5E). The T2A peptide allows separate expression of the 3V5-tagged ALD and 6HA-tagged GCD peptides, which was confirmed by immunoblot in the gametocytes (Fig. 5F). Using immunoprecipitation and immunoblot, the acetylation signal was detected for the 3V5-tagged ALD but not for the 6HA-tagged GCD in the *gcβ::T2A* gametocytes (Fig. 5G and H). These results demonstrated that GCβ is acetylated at the N-terminal ALD domain.

Sir2A catalyzes the deacetylation of GCβ in mature ookinete

To prove the function of Sir2A in deacetylating GCβ, we treated the *gcβ::6HA* gametocytes with nicotinamide (NAM, inhibitor of the sirtuin deacetylases) or trichostatin A (TSA, inhibitor of the HDAC deacetylases). NAM markedly promoted GCβ acetylation, whereas TSA did not influence GCβ acetylation (Fig. 6A), indicating that the deacetylase of GCβ is a member of the sirtuin family. Next, we examined GCβ acetylation alteration after loss of Sir2A during the gametocyte-zygote-ookinete development by comparing the *gcβ::6HA* and *gcβ::6HA*;Δ*sir2a* parasites. In gametocytes and zygotes, no noticeable changes in the acetylation level of GCβ were observed after loss of Sir2A (Fig. 6B). However, a significant increase in GCβ acetylation was detected in ookinetes of the *gcβ::6HA*;Δ*sir2a* compared to the *gcβ::6HA* (Fig. 6B). These results indicate that Sir2A is responsible for deacetylating GCβ in ookinetes.

We verified that GCβ deacetylation depends on the deacetylase activity of Sir2A. The conserved residue Glutamic acid (E) in the salt bridge of the sirtuin proteins is critical for the binding of substrate and that E to A mutation at this residue abolishes the protein function[37] (Fig. 6C). We replaced E195 with A in Sir2A of the *gcβ::6HA;sir2a::3V5* (*DTS1*) parasite and generated an enzymatically inactive mutant line designated *E195A* (Fig. 6C). The E195A substitution did not affect the protein level of Sir2A and GCβ in the ookinetes (Fig. 6D), but resulted in significantly increased GCβ acetylation in the ookinetes of *E195A* compared to the parental parasite *DTS1* (Fig. 6E). The functionally inactive protein of Sir2A-E195A lost localization at OES, correlating with the cytosolic distribution of the acetylated GCβ in ookinetes (Fig. 6F and G). These results in the *E195A* parasites are consistent with the mutually dependent localization of Sir2A and GCβ at OES in ookinete. The *E195A* ookinetes displayed severely impaired gliding motility compared to the *DTS1* counterpart (Fig. 6H) and developed no oocysts in the mosquitoes (Fig. 6I), resembling the phenotype of Sir2A disruption.

We tested the effect of pharmacological inhibition of Sir2A on GCβ deacetylation and localization in ookinetes. NAM is a product of the sirtuin-mediated catalysis, blocking protein deacetylation in a negative feedback[38]. The *gcβ::6HA* zygote culture was treated with NAM at different concentrations (Supplementary Fig. 5A). After 15 h treatment, NAM at 30 mM exerted a slight inhibition for ookinete development but influenced GCβ localization at OES in most of the developed ookinetes (Supplementary Fig. 5B and C). NAM at 30 mM did not affect the protein abundance of GCβ (Fig. 6J), but increased GCβ acetylation in the treated parasite culture (Fig. 6K). GCβ lost localization at OES in the NAM-treated ookinetes (GCβ polarization rate: 87.3 ± 6.0% in NAM, $n = 23$; 28.3 ± 9.5% in DMSO, $n = 28$) (Fig. 6L and M). NAM-treated ookinetes displayed severe defects in ookinete gliding (Fig. 6N), resembling the defect of Δ*sir2a* in Fig. 3I. Lastly, we evaluated the mosquito midgut transverse ability of the NAM-treated ookinetes. Mosquito infection with parasite was performed by membrane feeding the in vitro cultured ookinetes using a Hemotek system[39]. Compared to the DMSO-treated ookinetes, the NAM-treated ookinetes developed less number of oocysts in the midgut of mosquitoes on day 7 pi (Fig. 6O). These results indicated that during zygote to ookinete development, Sir2A deacetylates GCβ until ookinete maturation (Fig. 6P).

https://doi.org/10.1038/s41467-025-57517-y

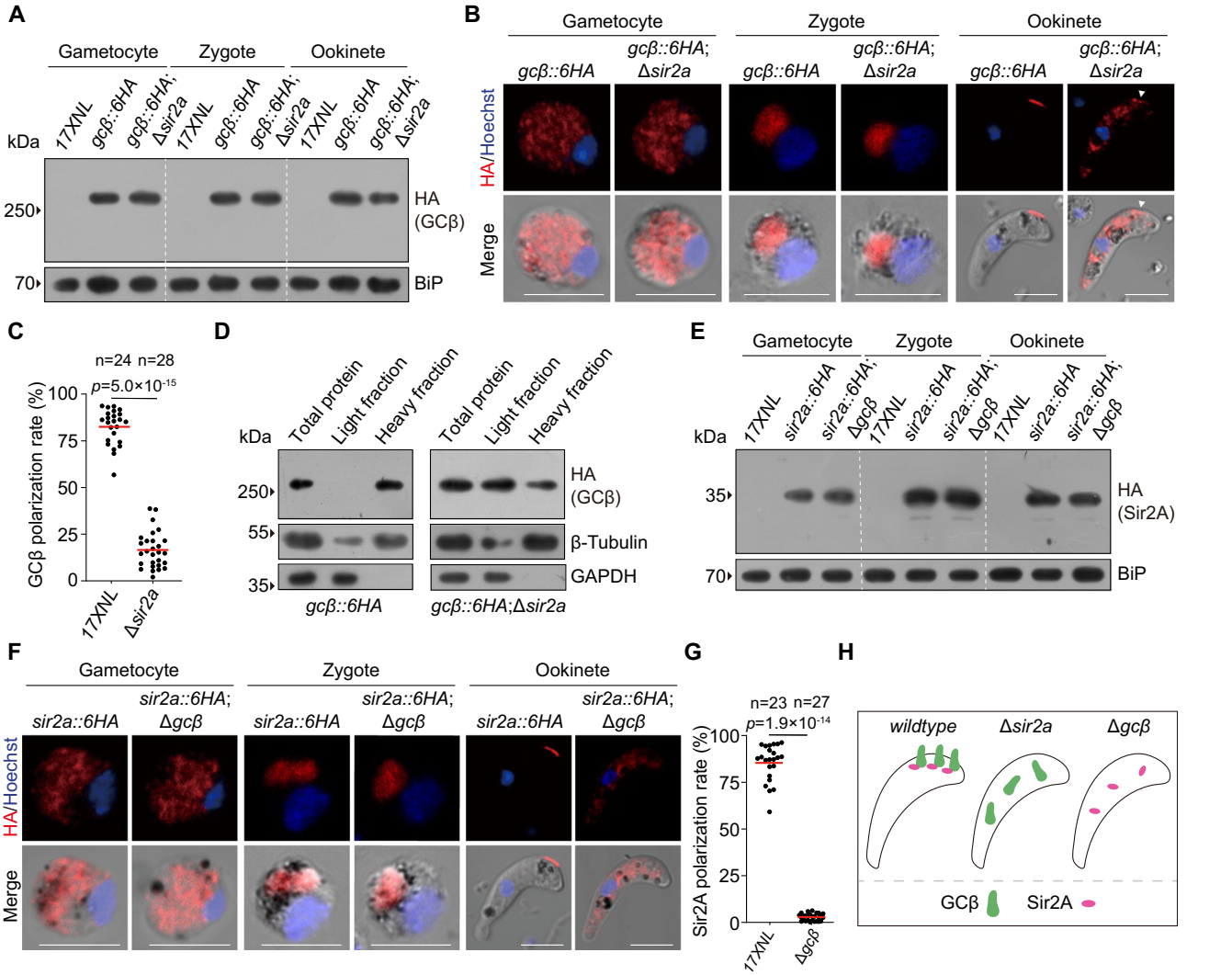

Fig. 4 | Mutual dependent localization of Sir2A and GCβ at OES in mature ookinete. A Immunoblot of HA-tagged GCβ in gametocytes, zygotes, and ookinetes of the 17XNL, *gcβ::6HA*, and *gcβ::6HA*;Δ*sir2a* parasites. BiP as a loading control. Representative for three independent experiments. **B** IFA of HA-tagged GCβ in gametocytes, zygotes, and ookinetes of the 17XNL, *gcβ::6HA*, and *gcβ::6HA*;Δ*sir2a* parasites. The white arrow indicates residual GCβ remaining at OES. Scale bar: 5 µm. Representative for three independent experiments. **C** Quantification of GCβ polarization level at OES in ookinetes in (**B**). n is the number of ookinetes analyzed. The red lines show the mean value. Two-sided Mann-Whitney *U* test. **D.** Cell fractionation analysis of GCβ in *gcβ::6HA* and *gcβ::6HA*;Δ*sir2a* ookinetes via immunoblot. Light fraction includes cytosolic proteins while heavy fraction includes membrane and cytoskeleton proteins. GAPDH is a cytosolic protein, and β-Tubulin is a cytoskeleton protein. Representative for two independent experiments. **E** Immunoblot of HA-tagged Sir2A in gametocytes, zygotes, and ookinetes of the 17XNL, *sir2a::6HA* and *sir2a::6HA*;Δ*gcβ* parasites. BiP as a loading control. Representative for three independent experiments. **F** IFA of HA-tagged Sir2A in gametocytes, zygotes, and ookinetes of the 17XNL, *sir2a::6HA* and *sir2a::6HA*;Δ*gcβ* parasites. Scale bar: 5 µm. Representative for three independent experiments. **G** Quantification of Sir2A polarization level at OES in ookinetes in (**F**). n is the number of ookinetes analyzed. The red lines show the mean value. Two-sided Mann-Whitney *U* test. **H** Cartoon showing mutual dependent localization of Sir2A and GCβ at OES in ookinete.

Elevated NAD$^+$ promotes GCβ deacetylation by Sir2A until ookinete maturation

Sir2A interacts with GCβ throughout the zygote to ookinete development, but GCβ is only deacetylated by Sir2A in mature ookinete. These observations imply temporal regulation of Sir2A activity for GCβ deacetylation during the ookinete development. NAD$^+$ is an essential co-substrate for sirtuin and the deacetylase activity requires a NAD$^+$ level exceeding the threshold[40]. Therefore, we examined whether the level of NAD$^+$ increases during the zygote to ookinete development and whether the elevated NAD$^+$ activates Sir2A to deacetylate GCβ. To monitor the intracellular NAD$^+$ dynamic during the zygote to ookinete development of *Plasmodium*, we used a genetically encoded NAD$^+$ fluorescent biosensor FiNad[41]. This sensor binds NAD$^+$ and significantly increases cpYFP fluorescence when cellular NAD$^+$ levels increase[41]. FiNad was fused with mCherry for dual-color ratiometric imaging of mCherry-FiNad[41] (Supplementary fig. 6A). mCherry-FiNad and mCherry-cpYFP (no NAD$^+$ sensing as negative control) were episomally expressed in the 17XNL parasites (Supplementary Fig. 6B). Both cpYFP (detecting NAD$^+$) and mCherry (for expression normalization) were detected in the cytoplasm from gametocyte to ookinete for parasites expressing either mCherry-FiNad or mCherry-cpYFP (Supplementary Fig. 6C). The cpYFP/mCherry ratio indicating the level of NAD$^+$ did not significantly change from gametocyte to zygote in parasites expressing mCherry-FiNad. However, the ratio increased markedly during the zygote-to-ookinete development, reaching a maximal signal in mature ookinetes (Fig. 7A and B and Supplementary Fig. 6D and E). As expected, the cpYFP/mCherry ratio from mCherry-cpYFP showed no obvious fluorescence changes from gametocyte to ookinete (Fig. 7A and B and Supplementary Fig. 6D and E). These results indicated that the

https://doi.org/10.1038/s41467-025-57517-y

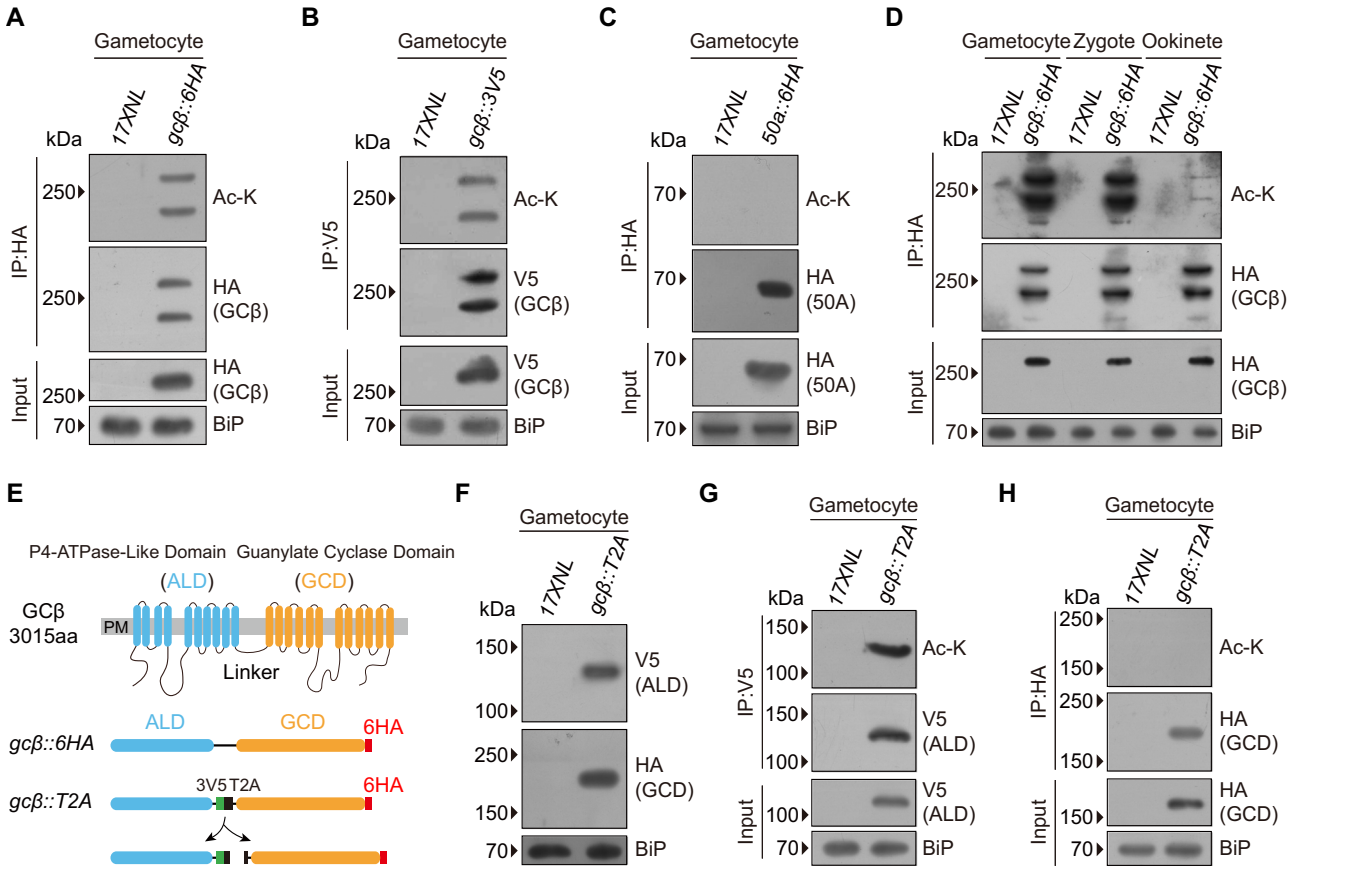

Fig. 5 | GCβ is acetylated at gametocytes and deacetylated at mature ookinetes. **A** Detection of GCβ acetylation in 17XNL and *gcβ::6HA* gametocytes. HA-tagged GCβ was immunoprecipitated using an anti-HA antibody, and the precipitates were analyzed using an anti-acetyl-lys antibody (Ac-K). BiP as a loading control. Representative for three independent experiments. **B** Detection of GCβ acetylation in 17XNL and *gcβ::3V5* gametocytes. V5-tagged GCβ was immunoprecipitated using anti-V5 antibody, and the precipitates were analyzed using Ac-K. Representative for three independent experiments. **C** Detecting of CDC50A acetylation in 17XNL and *cdc50a::6HA* gametocytes. HA-tagged CDC50A was immunoprecipitated using an anti-HA antibody, and the precipitates were analyzed using Ac-K. Representative for three independent experiments. **D** GCβ acetylation dynamics in gametocytes, zygotes, and ookinetes of 17XNL and *gcβ::6HA* parasites. HA-tagged GCβ was immunoprecipitated using an anti-HA antibody, and the precipitates were analyzed using Ac-K. Representative for three independent experiments. **E** Diagram of the *gcβ::T2A* line with a T2A peptide inserted into the linker region of endogenous GCβ in *gcβ::6HA* parasite. T2A allows separated expression of the V5-tagged ALD (P4-ATPase-like domain) and HA-tagged GCD (guanylate cyclase domain) of GCβ. **F** Immunoblot confirming separated expression of V5-tagged ALD and HA-tagged GCD in *gcβ::T2A* gametocytes. Representative for three independent experiments. **G** Detecting of acetylation in ALD of GCβ in *gcβ::T2A* gametocytes. V5-tagged ALD was immunoprecipitated using anti-V5 antibody, and the precipitates were analyzed using Ac-K. Representative for three independent experiments. **H** Detecting of acetylation in GCD of GCβ in *gcβ::T2A* gametocytes. HA-tagged GCD was immunoprecipitated using an anti-HA antibody, and the precipitates were analyzed using Ac-K. Representative for three independent experiments.

level of NAD^+ increases during zygote to ookinete development and accumulates to its maximum in mature ookinetes.

Next, we depleted the intracellular NAD^+ to analyze its effect on GCβ deacetylation by Sir2A during the zygote to ookinete development. In the *Plasmodium*, the NAD^+ homeostasis relies heavily on the nicotinamidase for NAD^+ biosynthesis[42,43]. Chemical inhibition of nicotinamidase by an inhibitor 5-Me-Nicotinaldehyde (5-Me) caused significant depletion of intracellular NAD^+ in the asexual blood stage of *P. falciparum*[43]. We tested the effect of 5-Me treatment on the level of NAD^+ during the zygote to ookinete development in *P. yoelii*. The 17XNL zygote culture was treated with 5-Me or DMSO (Supplementary Fig. 6F). Compared to DMSO, 5-Me treatment inhibited the increase of cpYFP fluorescence from mCherry-FiNad during zygote to ookinete development (Fig. 7C and D). In the parallel experiments, the parasites expressing mCherry-cpYFP showed no obvious fluorescence changes during ookinete development after either 5-Me or DMSO treatment (Fig. 7C and D). These results indicated that 5-Me treatment decreases the NAD^+ biosynthesis during zygote to ookinete development and depletes the NAD^+ content in mature ookinetes. 5-Me resulted in a slight inhibition for ookinete development after 15 h treatment (Fig. 7E). The drastic reduction in NAD^+ levels after 5-Me treatment increased GCβ acetylation in the treated ookinete culture (Fig. 7F) and influenced GCβ localization at OES in the developed ookinetes (Fig. 7G and H). Compared to the DMSO-treated ookinetes, the 5-Me-treated ookinetes displayed defects in the ookinete gliding (Fig. 7I). These results suggested that during zygote to ookinete development, the elevated level of NAD^+ may reach the threshold to activate Sir2A for deacetylating GCβ until ookinete maturation.

Discussion

Our previous study revealed that during the zygote to ookinete development, the GCβ/CDC50A complex translocates from the cytoplasm to OES until ookinete maturation. By GCβ/CDC50A polarization at OES for elevating local cGMP concentration, mature ookinetes can activate cGMP signaling and initiate gliding motility. In this study, we identified Sir2A which forms a complex with GCβ/CDC50A during the zygote to ookinete development. Sir2A displays localization at OES in mature ookinetes similarly to GCβ/CDC50A. Notably, GCβ is acetylated in the gametocyte and maintains the acetylated status during the ookinete development. Upon reaching

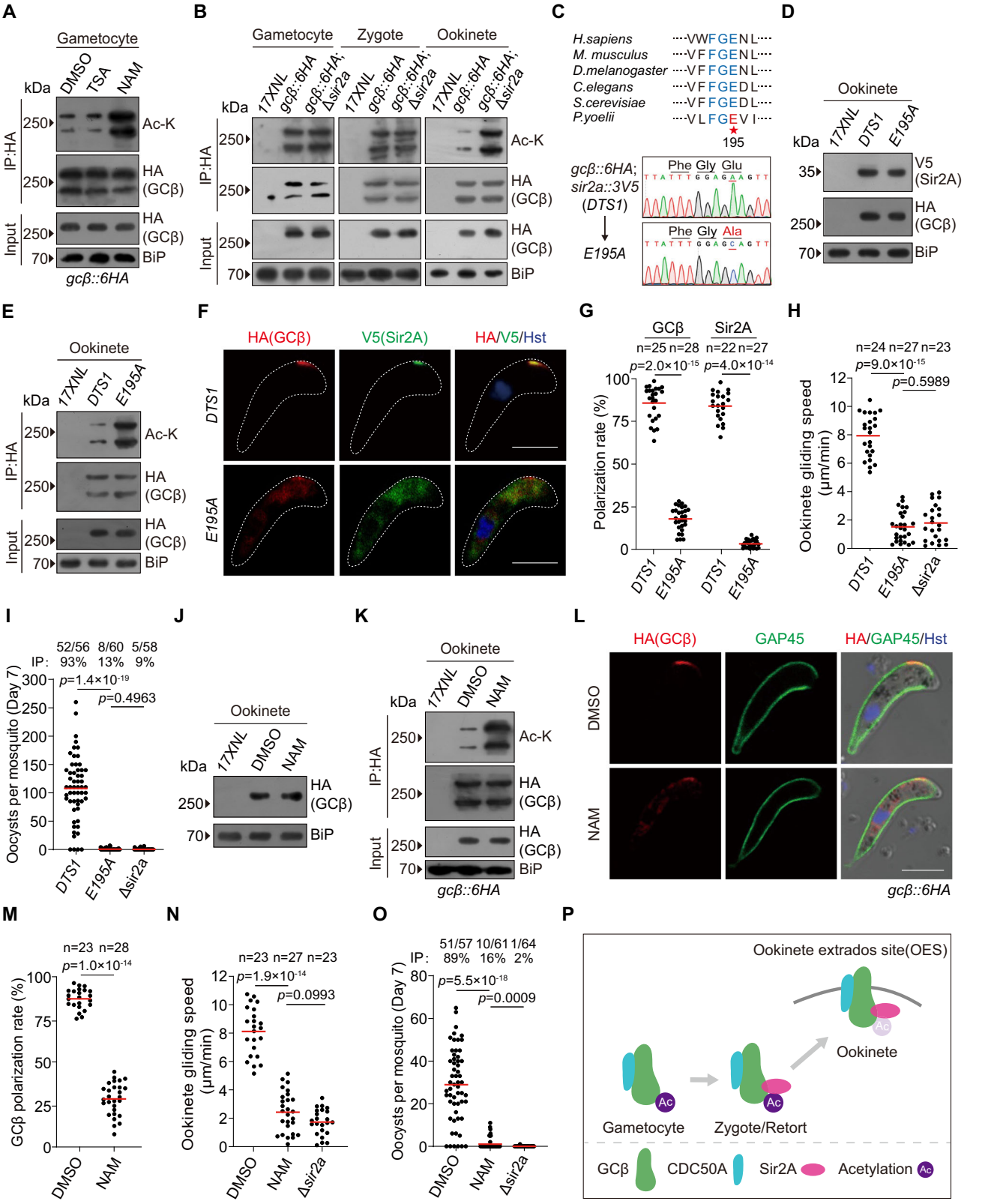

ookinete maturation, GCβ is deacetylated by Sir2A in the complex. Deacetylated GCβ, accompanied by CDC50A and Sir2A in the complex, translocates from the cytoplasm to OES for initiating the cGMP signal. Furthermore, we revealed that the intracellular NAD^+ increases during the zygote to ookinete development and reaches a maximum level in mature ookinete. The elevated NAD^+ levels in mature ookinetes induce the Sir2A-dependent GCβ deacetylation and facilitate OES translocation. We proposed a working model in Supplementary Fig. 7.

The *Plasmodium* parasites encode two sirtuin proteins Sir2A and Sir2B, which are conserved among different *Plasmodium* species[29]. Two previous studies successfully knocked out the *sir2a* gene in *P. falciparum*[30,31], indicating a nonessential function for in vitro parasite proliferation during asexual blood stages. However, Sir2A was found to

Fig. 6 | Sir2A catalyzes the deacetylation of GCβ in mature ookinete. A Detection of GCβ acetylation in *gcβ::6HA* gametocytes treated with deacetylase inhibitors TSA or NAM. HA-tagged GCβ was immunoprecipitated using an anti-HA antibody, and the precipitates were analyzed using Ac-K. BiP as a loading control. Representative for three independent experiments. **B** GCβ acetylation dynamics during the gametocyte-zygote-ookinete development of 17XNL, *gcβ::6HA*, and *gcβ::6HA;Δsir2a* parasites. Representative for three independent experiments. **C** Generation and characterization of the mutant parasite with E195 replaced with alanine (**A**) in endogenous Sir2A from the parental parasite *gcβ::6HA;sir2a::3V5* (*DTS1*). Conserved glutamic acid (**E**, red star) in sirtuin proteins from several organisms is indicated. DNA sequencing confirming E195A substitution in the resulting mutant clone *E195A*. **D** Immunoblot of HA-tagged GCβ and V5-tagged Sir2A in *DTS1* and *E195A* ookinetes. Representative for three independent experiments. **E** Detection of GCβ acetylation in 17XNL, *DTS1*, and *E195A* ookinetes. HA-tagged GCβ was immunoprecipitated using an anti-HA antibody, and the precipitates were analyzed using Ac-K. Representative for three independent experiments. **F** IFA of HA-tagged GCβ and V5-tagged Sir2A in *DTS1* and *E195A* ookinetes. Scale bar: 5 μm. Representative for two independent experiments. **G** Quantification of GCβ and Sir2A polarization level at OES in ookinetes in (**F**). n is the number of ookinetes analyzed. The red lines show the mean value. Two-sided Mann-Whitney *U* test. **H** Ookinete gliding motility. n is the number of ookinetes analyzed. The red lines show the mean value. Two-sided Mann-Whitney *U* test. Representative for three independent experiments. **I** Midgut oocyst formation in mosquitoes at day 7 post-infection. Red lines show the mean value, two-sided Mann-Whitney *U* test. x/y on the top is the number of mosquitoes containing oocyst/the number of mosquitoes dissected. The percentage represents the infection prevalence of mosquitoes. Representative for two independent experiments. **J** Immunoblot of HA-tagged GCβ in *gcβ::6HA* ookinetes after DMSO or NAM treatment. Representative for three independent experiments. **K** Detection of GCβ acetylation in *gcβ::6HA* ookinetes after DMSO or NAM treatment. Representative for three independent experiments. **L** IFA of HA-tagged GCβ in DMSO- or NAM-treated *gcβ::6HA* ookinetes. GAP45 is an IMC marker. Scale bar: 5 μm. Representative for three independent experiments. **M** Quantification of GCβ polarization level at OES in ookinetes in (**I**). n is the number of ookinetes analyzed. The red line shows the mean value. Two-sided Mann-Whitney *U* test. **N** Ookinete gliding motility of the DMSO- or NAM-treated *gcβ::6HA* ookinetes. n is the number of ookinetes analyzed. The red line shows the mean value. Two-sided Mann-Whitney *U* test. Representative for three independent experiments. **O** Midgut oocyst formation in mosquitos at day 7 post-infection. Mosquito infection with the NAM-treated ookinetes was performed by membrane feeding using a Hemotek system. The red lines show the mean value. Two-sided Mann-Whitney *U* test. x/y on the top is the number of mosquitoes containing oocyst/the number of mosquitoes dissected. The percentage number is the mosquito infection prevalence. Representative for three independent experiments. **P** A model showing GCβ deacetylation by Sir2A for OES localization until ookinete maturation during ookinete development.

modulate the transcription of the *var* gene family by regulating the acetylation status of nuclear histones in the asexual blood stages of *P. falciparum*[30]. Whether Sir2A exerts functions in other parasite stages has not yet been investigated. In this study, we used TurboID-based proximity labeling to search the GCβ-interacting proteins in the ookinetes of the rodent malaria parasite *P. yoelii*. Among the 251 interacting proteins yielded by quantitative mass spectrometry, Sir2A was the top significant hit, but Sir2B was not detected. Unlike the asexual blood stage expression of Sir2A in *P. falciparum*, the expression of Sir2A was not detected or extremely low in the asexual blood stage in *P. yoelii*. The *var* gene family is unique to *P. falciparum*, and no homologs of the *var* gene family exist in the genome of *P. yoelii*[44], which is consistent with the lack of Sir2A expression in the asexual blood stage proliferation of *P. yoelii*. In mature ookinetes, Sir2A is not localized at nuclei but displayed complete concentration at OES (Figs. 1D, 1F, 1H, and 2A). Sir2A forms a complex with GCβ, catalyzes GCβ deacetylation, and regulates GCβ translocation from cytoplasm to OES during the ookinete development. Besides the canonical pair of Sir2A-Histone in *P. falciparum*[30], Sir2A-GCβ in the ookinetes represents a new sirtuin-substrate pair discovered in the *Plasmodium* parasites.

In a recent reverse genetic screen in *P. berghei*, Ukegbu et al characterized a transmembrane protein STONES associated with OES and required for ookinete motility[45]. Interestingly, the homolog protein of STONES in *P. yoelii* was included in the list of proteins identified by TurboID-based proximity labeling of GCβ in this study (Supplementary Data 1). To date, the component proteins localizing at OES in ookinete include GCβ, CDC50A, Sir2A, and STONES, although more proteins may be discovered.

Acetylation and deacetylation are reversible protein post-translational modifications that regulate protein stabilization, enzymatic activity, localization, and protein-protein interaction[24]. Recently, the importance of protein acetylation and deacetylation in *Plasmodium* has been recognized, including the asexual blood stage proliferation and gametocytogenesis[46–50]. Our study demonstrates that GCβ is acetylated in the female gametocyte and remains acetylated during the ookinete development. Until ookinete maturation, the deacetylation of GCβ directs the protein translocation from cytoplasm to OES and initiates gliding of mature ookinetes. Two possible mechanisms may explain the effect of deacetylation in GCβ localization at OES in mature ookinete. First, a high level of acetylation in GCβ may negatively affect the trafficking of the GCβ-CDC50A-Sir2A complex from cytoplasm to OES. Second, a low level of acetylation facilitates GCβ anchoring with PPM at the OES.

The *P. yoelii* GCβ is a 3015 aa protein containing 22 transmembrane helixes. Previous transcriptome studies detected a low transcript level of *gcβ* in female gametocytes of *P. berghei* and *P. yoelii*[51,52]. Currently, it is difficult to purify enough endogenous GCβ protein from gametocytes for mass spectrometry analysis of the acetylated lysine in GCβ. Alternatively, we used a previously generated parasite line *gcβ::T2A* in which the 3V5-tagged ALD and 6HA-tagged GCD were separately expressed in the gametocytes. In the *gcβ::T2A* gametocytes, we detected the acetylation in the 3V5-tagged ALD peptide but not in the 6HA-tagged GCD peptide, indicating that the potential acetylated lysine exists in ALD (1-1248 aa) of GCβ. In future studies, it is important to characterize the acetylated lysine residues in ALD. GCβ is a structurally unusual protein in which the C-terminal GCD is thought to be responsible for cGMP synthesis, but the N-terminal ALD is functionally obscure. GCβ is acetylated at ALD, and deacetylation of ALD plays a critical role in GCβ translocation from cytoplasm to OES in mature ookinetes. However, the separated ALD is distributed in the cytoplasm and is not targeted to OES in mature ookinetes of the *gcβ::T2A* parasites[19]. These results suggest that both the deacetylation and structural integrity of protein are required for GCβ translocation from cytoplasm to OES during ookinete development.

Sir2A interacts with its substrate protein GCβ throughout ookinete development but catalyzes GCβ deacetylation until ookinete maturation, implying temporal regulation of Sir2A activity during the ookinete development. NAD^+ functions as a cofactor or substrate for hundreds of enzymes[53,54] and plays important roles in many cellular processes[55,56]. The deacetylase activity of sirtuin requires an appropriate level of NAD^+[40]. Our study revealed that the level of NAD^+ increases during the ookinete development and reaches a maximum upon ookinete maturation. The NAD^+ accumulating to exceed the threshold functions as a signal turning on Sir2A activity for Sir2A-dependent GCβ deacetylation. In this study, the functional link between NAD^+, Sir2A activity, and GCβ deacetylation is currently correlative and would require further investigation to ascertain it at the molecular level. Consistent with this, in model organism lifespan-extending metabolic manipulations, such as physical exercise, caloric restriction, and time-restricted feeding, function in part by increasing NAD^+ levels and activating sirtuins[57,58]. NAD^+ was first discovered by regulating the metabolism in yeast[56], and thus the links between NAD^+ and metabolism have been widely investigated[59,60]. In *Plasmodium*,

https://doi.org/10.1038/s41467-025-57517-y

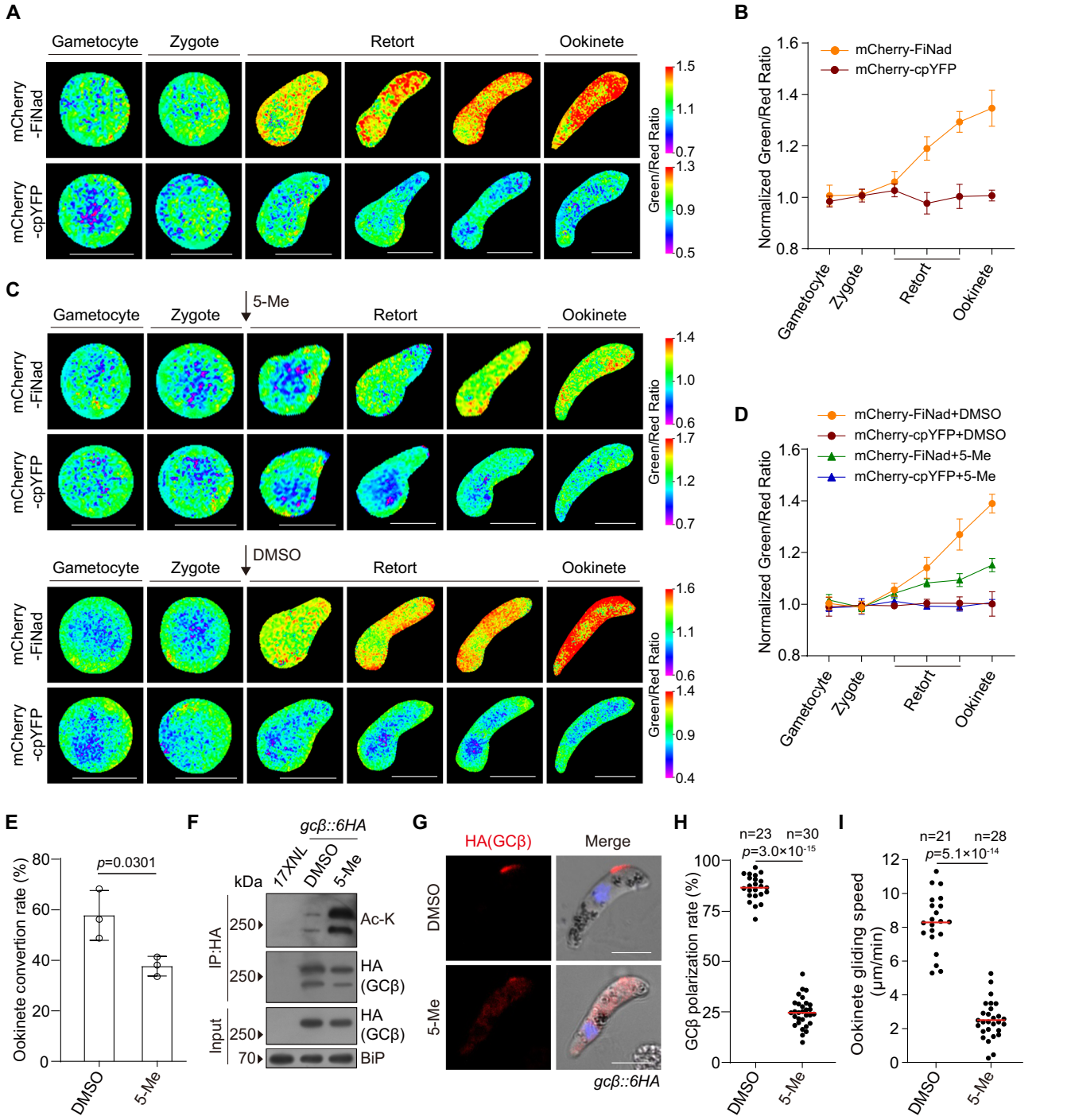

Fig. 7 | Elevated NAD⁺ promotes GCβ deacetylation by Sir2A until ookinete maturation. A Detection of the NAD⁺ dynamics during gametocyte to ookinete development. The 17XNL parasites were transfected with the NAD⁺ fluorescent biosensor mCherry-FiNad (detailed information in Supplementary Fig. 6). mCherry-cpYFP is a negative control sensing no NAD⁺. The cytoplasmic fluorescence of both cpYFP (488 nm for NAD⁺ detection) and mCherry (555 nm for normalization) were recorded. The ratio between cpYFP and mCherry indicates the NAD⁺ level. Scale bar: 5 μm. Representative for three independent biological replicates. **B** Quantification of the cpYFP/mCherry ratio in (**A**). The ratio in gametocytes was set as 1.0, and all ratios in other stages were normalized. Means ± SD ($n = 3$ biological replicates). 30 cells were analyzed in each group of each replicate (detailed information in Supplementary Fig. 6D and E). **C** The NAD⁺ dynamics during ookinete development treated with the nicotinamidase inhibitor 5-Me-Nicotinaldehyde (5-Me). 5-Me or DMSO was added to the ookinete culture at the zygote stage (black arrow) for the parasites expressing Cherry-FiNad or Cherry-cpYFP. Scale bar: 5 μm. Representative for three independent biological replicates. **D** Quantification of the cpYFP/mCherry ratio in (**C**). Means ± SD ($n = 3$ biological replicates). 30 cells were analyzed in each group of each replicate. **E** In vitro mature ookinete formation of parasites treated with 5-Me or DMSO. Mean ± SD from three independent experiments, two-tailed t test. **F** Detection of GCβ acetylation in *gcβ::6HA* ookinetes treated with 5-Me or DMSO. HA-tagged GCβ was immunoprecipitated using an anti-HA antibody, and the precipitates were analyzed using Ac-K. Representative for three independent experiments. **G** IFA of HA-tagged GCβ in *gcβ::6HA* ookinetes treated with 5-Me or DMSO. Scale bar: 5 μm. Representative for two independent experiments. **H** Quantification of GCβ polarization level at OES in ookinetes in (**G**). n is the number of ookinetes analyzed. The red lines show the mean value. Two-sided Mann-Whitney U test. **I** Ookinete gliding motility of the 5-Me- or DMSO-treated *gcβ::6HA* ookinetes. n is the number of ookinetes analyzed. The red lines show the mean value. Two-sided Mann-Whitney U test. Representative for two independent experiments.

elevated NAD^+ levels during ookinete development may prepare for enhanced oxidative metabolism requirements in the upcoming ookinete gliding. The synthesis of intracellular NAD^+ is dictated by the de novo synthesis pathway or salvage pathway[56]. In *Plasmodium*, there is only a salvage pathway[42]. In the future, it will be interesting to elucidate whether the increase of NAD^+ levels is caused by the increase of enzyme expression or activity in the NAD^+ salvage pathway during ookinete development.

Methods

Mice and mosquitoes usage and ethics statement

The animal experiments conducted in this study were approved by the Committee for Care and Use of Laboratory Animals of Xiamen University (XMULAC20220287). Female ICR mice (5 to 6 weeks old) were obtained from the Animal Care Center of Xiamen University and used for parasite propagation, drug selection, parasite cloning, and mosquito feeding. The larvae of *Anopheles stephensi* mosquitoes (*Hor* strain) were reared at 28 °C, 80% relative humidity, and a 12 h light/12 h dark condition in a standard insect facility. Adult mosquitoes were supplemented with 10% (w/v) sugar solution containing 0.05% 4-aminobenzoic acid and kept at 23 °C.

Plasmid construction and parasite transfection

The parasite CRISPR/Cas9 plasmid pYCm was used for gene editing[33,61]. To construct vectors for gene deletion, the 5′ and 3′ genomic fragments (400–800 bp) of the target gene were amplified as the left and right homologous templates respectively, and inserted into the pYCm vector. To construct vectors for gene tagging, the 5′- and 3′- flanking sequences (400–800 bp) at the designed insertion site of target genes were amplified as the left and right homologous templates respectively. DNA fragments encoding 6HA or 3V5 were inserted between the homologous templates in the frame with the coding sequence of the target gene. To construct vectors for nucleotide replacement, the homologous template comprises a DNA fragment spanning 582 bp upstream and 249 bp downstream of the target nucleotide in the *sir2a* gene. At least two sgRNAs were designed for each modification using the online program EuPaGDT (http://grna.ctegd.uga.edu/). Paired oligonucleotides for sgRNA were denatured at 95 °C for 3 min, annealed at room temperature for 5 min, and ligated into pYCm. The sequences of primers and oligonucleotides used in this study are listed in Supplementary Table 1. The schizont-infected erythrocytes were isolated from infected mice for parasite electroporation using a 60% Nycodenz density gradient centrifugation. Parasites were electroporated with 5 μg plasmid using a Nucleofector 2b Device (Lonza, Germany). Transfected parasites were immediately intravenously injected into a naïve mouse and exposed to pyrimethamine (6 mg/mL) provided in mouse drinking water 24 h after injection.

Genotyping of genetically modified parasites

All genetically modified parasites (listed in Supplementary Table 2) were generated from the *P. yoelii* 17XNL or 17XNL-derived parasite lines. 10 μL parasite-infected blood samples were collected from the infected mice tail vein and lysed using 1% saponin in PBS. After centrifugation at 13,000 × *g* for 5 min, the pellets were washed twice with PBS, boiled at 95 °C for 10 min, and centrifuged at 13,000 × *g* for 5 min. Supernatants containing parasite genomic DNA were subjected to genotyping. For each gene modification, the 5′ and 3′ homologous recombination events were detected by diagnostic PCR, confirming the successful integration of homologous templates (Supplementary Fig. 8). Parasite clones with targeted modifications were obtained by limiting dilution cloning. At least two clones of each gene-modified parasite were used for phenotypic analysis. Modified parasite clones subject to additional modification were negatively selected to remove the pYCm plasmid. Mice infected with pYCm plasmid-carrying parasites were exposed to 5-Fluorocytosine (Sigma-Aldrich, cat#F6627) in drinking water (2.0 mg/mL) for 6–8 days. After negative selection, two pairs of pYCm-specific primers are used to survey the residual plasmids. Clearance of plasmid in parasites after negative selection was confirmed by checking the parasite survival after reapplying pyrimethamine pressure (6 μg/mL) in mice.

Parasite asexual blood stage proliferation in mouse

Four ICR mice were included in each group. After intravenous injection of 1.0×10^5 parasites, parasite proliferation was monitored by Giemsa-stained thin blood smears every 2 days from day 2 to 14 post-infection. The parasitemia was calculated as the ratio of parasitized erythrocytes over total erythrocytes.

Gametocyte induction in mouse

ICR mice were treated with phenylhydrazine (80 μg/g mouse body weight; Sangon Biotech, China, cat#A600705-0025) via intraperitoneal injection. Three days post-injection, the mice were infected with 5.0×10^6 parasites through intravenous injection. Gametocytemia usually peaks at day 3 post-infection. Male and female gametocytes were counted after Giemsa-stained thin blood smears. Male or female gametocytemia was calculated as a percentage of the number of male or female gametocytes over the number of parasitized erythrocytes.

Gametocyte purification

Gametocytes were purified using the method described previously[62]. ICR mice were intraperitoneally treated with phenylhydrazine 3 days before parasite infection. From day 3 post parasite infection, the mice were orally administered 0.12 mg/day of sulfadiazine (Sigma-Aldrich, cat#S8626) for 2 days to eliminate asexual blood stage parasites. Approximately 1 mL of gametocyte-containing mouse blood was collected from the orbital sinus and suspended in 6 mL gametocyte maintenance buffer (GMB, 137 mM NaCl, 4 mM KCl, 1 mM $CaCl_2$, 20 mM glucose, 20 mM HEPES, 4 mM $NaHCO_3$, 0.1% BSA, and pH 7.2), the 7 mL parasite sample was layered on top of a 2 mL 48% Nycodenz solution (27.6% w/v Nycodenz in 5 mM Tris-HCl, 3 mM KCl, 0.3 mM EDTA, and pH 7.2) in a 15 mL Falcon tube. After centrifugation at 1900 × *g* for 20 min, the gametocytes were collected from the interface layer and washed twice with GMB for further use.

Male gametocyte exflagellation assay

2.5 μL of gametocyte-containing mouse blood was mixed with 100 μL of exflagellation medium. The exflagellation medium was composed of RPMI 1640 medium supplemented with 100 μM xanthurenic acid (XA, Sigma-Aldrich, cat#D120804), 2 unit/mL heparin, and pH 7.4. The mixture was incubated at 22 °C for 10 min. The number of parasite exflagellation centers (ECs) and total red blood cells were counted within a 1 × 1 mm square area of a hemocytometer under the light microscope. The exflagellation rate was calculated as the number of ECs per 100 male gametocytes.

In vitro ookinete culture and purification

Mouse blood carrying 6–10% gametocytemia was collected and mixed with ookinete culture medium (RPMI 1640, 10% FCS, 100 μM XA, 25 mM HEPES, 100 μg/mL streptomycin, 100 U/mL penicillin, and pH 8.0). The culture was put at 22 °C for 12–15 h for gametogenesis, fertilization, and ookinete development. Ookinetes formation was evaluated based on cell morphology in Giemsa-stained thin blood smears. The mature ookinete conversion rate was calculated as the number of crescent-shaped mature ookinete (stage V) over that of total ookinetes (from stage I to V). Mature ookinete was purified using Nycodenz density gradient centrifugation as described previously[63]. After centrifugation at 500 × *g* for 5 min, ookinete pellets were resuspended with 7 mL PBS and transferred onto the top of 2 mL of 63% Nycodenz in a 15 mL Falcon tube. After centrifuging at 1000 × *g* for 20 min, the interface layer enriched with ookinetes was collected from the tube.

The purity of ookinetes was examined by hemocytometer analysis. Ookinetes with more than 80% purity were used for further experiments.

Parasite infection in mosquito

100 female *Anopheles stephensi* mosquitoes were allowed to feed on an anesthetized mouse with 4–6% gametocytaemia for 30 min. To evaluate midgut infection of the parasite, 30 mosquitoes were dissected, and the midguts were stained with 0.1% mercurochrome 7 days post feeding. The number of oocysts in each midgut was counted under the microscope. For quantifying salivary gland sporozoites, the salivary glands were dissected from mosquitoes 14 days after feeding. Sporozoites from 30 mosquitoes were counted using a hemocytometer, and the average number of sporozoites per mosquito was calculated.

Mosquito membrane feeding with ookinetes

1.0×10^7 purified ookinetes from the culture were mixed with 1 mL of naïve mouse blood. The ookinete and blood mixture were added to the membrane feeder and fed to 60 female mosquitoes for 30 min using the Hemotek (6W1, Hemotek Limited, England). Fully engorged mosquitoes were transferred to the new container and maintained under standard conditions after feeding. 30 mosquitoes were dissected and the midguts were stained with 0.1% mercurochrome 7 days post feeding, the number of early oocysts in each midgut was counted under the microscope.

Ookinete gliding assay

All procedures were performed in a temperature-controlled room at 22 °C. 20 µL of the suspended ookinete cultures were mixed with 20 µL of Matrigel (BD Biosciences, cat#356234) on ice. The ookinete and Matrigel mixtures were transferred onto a slide, covered with a coverslip, and sealed with nail varnish. The slide was rested for 30 minutes before observation under the microscope. After tracking a gliding ookinete under the microscope, time-lapse videos (1 frame per 20 s, for 20 min) were taken to track ookinete movement using a Nikon ECLIPSE E100 microscope fitted with an ISH500 digital camera controlled by ISCapture v3.6.9.3 N software (Tucsen). Ookinete motility speeds were calculated with ImageJ software using the MtrackJ plugin[64].

Antibodies and antiserum

The primary antibodies included: rabbit anti-HA (Cell Signaling Technology, cat#3724S, 1:1000 for immunoblot (IB), 1:1000 for immunofluorescence (IF), 1:1000 for immunoprecipitation (IP)), rabbit anti-acetylated Lys (Cell Signaling Technology, cat#9441, 1:1000 for IB), mouse anti-HA (Cell Signaling Technology, cat#2367S, 1:500 for IF), mouse anti-V5 (GenScript, A01724-100, 1:1000 for IF, 1:1000 for IB, 1:1000 for IP), mouse anti-α-tubulin II (Sigma-Aldrich, cat#T6199, 1:1000 for IF), mouse anti-β-tubulin (Sigma-Aldrich, cat#T5201, 1:1000 for IB), mouse anti-GAPDH (Servicebio, cat#GB12002, 1:1000 for IB), mouse anti-Myc (Cell Signaling Technology, cat#2276S, 1:1000 for IF, 1:1000 for IB). The secondary antibodies included: HRP-conjugated goat anti-rabbit IgG (Abcam, cat#ab6721, 1:5000 for IB), HRP-conjugated goat anti-mouse IgG (Abcam, cat#ab6789, 1:5000 for IB), Alexa 555 goat anti-rabbit IgG (ThermoFisher Scientific, cat#A21428, 1:1000 for IF), Alexa 488 goat anti-mouse IgG (ThermoFisher Scientific, cat#A11001, 1:1000 for IF), Alexa 488 conjugated streptavidin (Invitrogen, S32354, 1:1000 for IF). The anti-serums included rabbit anti-P28 (our lab, 1:1000 for IF), rabbit anti-BiP (our lab, 1:1000 for IB), and rabbit anti-GAP45 (our lab, 1:1000 for IF).

Immunofluorescence assay

Parasites fixed in 4% paraformaldehyde were transferred to a Poly-L-Lysine coated coverslip in a 24-well plate and centrifuged at 550 × *g* for 5 min. Parasites were then permeabilized with 0.1% Triton X-100 solution in PBS for 10 minutes, blocked in 5% BSA solution in PBS for 60 min at room temperature, and incubated with the primary antibodies diluted in 5% BSA-PBS for 1 h at room temperature. After three washes with PBS, the coverslip was incubated with fluorescent conjugated secondary antibodies for 1 hat at room temperature. Cells were stained with Hoechst 33342, mounted in 90% glycerol solution, and sealed with nail varnish. All images were acquired and processed using identical settings on Zeiss LSM 880 or LSM 980 confocal microscopes.

Protein extraction and immunoblot

Protein extracts from the asexual blood stage parasites, gametocytes, and ookinetes were lysed in buffer A (0.1% SDS, 1 mM DTT, 50 mM NaCl, 20 mM Tris-HCl, and pH 8.0) supplemented with protease inhibitor cocktail (Medchem Express, cat#HY-K0010) and PMSF (Roche, cat#10837091001). After ultrasonication, the extracts were incubated on ice for 30 min followed by centrifugation at 12,000 × *g* for 10 min*utes* at 4 °C. The supernatant was lysed in 1 × Laemmli sample buffer. After SDS-PAGE separation, samples were transferred to the PVDF membrane (Millipore, cat#IPVH00010). The membrane was blocked with 5% skim milk, probed with primary antibodies for 1 hat room temperature, rinsed 3 times with 1 × TBST (20 mM Tris-HCl pH 7.5, 150 mM NaCl, and 0.1% Tween20), and incubated with HRP-conjugated secondary antibodies. After three washes with TBST, the membrane was visualized with enhanced chemiluminescence detection (Advansta, cat#K12045-D10).

Cellular fractionation

Cellular fractionation was conducted as described previously[19]. Purified ookinetes were ruptured in the hypotonic buffer (10 mM HEPES, 10 mM KCl, and pH 7.4) after passing through a 1 mL syringe needle gently ten times. The total cell lysate was centrifuged for 15 minat 1000 × *g*. The supernatant (light fraction, including cytoplasm and cytosol vesicles) and the pellet (heavy fraction, including the plasma membrane, IMC, and cytoskeleton) were collected and solubilized in 1 × Laemmli sample buffer for 10 minutes on ice. The solubilized protein samples were analyzed using immunoblot.

Protein immunoprecipitation

Parasites were lysed in buffer A plus (0.01% SDS, 1 mM DTT, 50 mM NaCl, 20 mM Tris-HCl, and pH 8.0) with protease inhibitor cocktail and PMSF, centrifuged at 12,000 × g for 10 min at 4 °C before collecting the supernatant solution. Rabbit anti-HA antibody was added to the protein solution and incubated at 4 °C for 12 h on a vertical mixer. After incubation, 20 µL protein A/G beads (Pierce, cat#20423) pre-balanced with buffer A plus were added and incubated for 2 h. The beads were washed three times with buffer A plus, mixed with an equal volume of 2 × Laemmli sample buffer, and oscillated on Vortex at 500 g for 5 minutes. All samples were centrifuged at 12,000×g for 5 minutes. An equal volume of supernatant from each sample was used for immunoblot.

Detection of protein acetylation

Parasite cells were lysed in buffer A plus (0.01% SDS, 1 mM DTT, 50 mM NaCl, 20 mM Tris-HCl, and pH 8.0) containing protease inhibitor cocktail, PMSF and 30 mM NAM, incubated on ice for 30 minutes, and centrifuged at 12,000 × *g* for 10 minutes at 4 °C before collecting the supernatant solution. Rabbit anti-HA antibody was added to the protein solution and incubated at 4 °C for 12 h on a vertical mixer. After incubation, 20 µL protein A/G beads pre-balanced with buffer A plus were added and incubated for 2 h. The beads were washed three times with buffer A plus, mixed with an equal volume of 2 × Laemmli sample buffer, and oscillated at 500 g for 5 minutes. All samples were centrifuged at 12,000 g for 5 minutes. An equal volume of supernatant from each sample were used for immunoblot. Protein acetylation was analyzed using Rabbit anti-acetylated Lys antibody.

Protein proximity labeling and biotinylated protein pull-down

1.0×10^8 purified ookinetes from the *gcβ::TurboID::6HA* and *gcβ::T2A::TurboID::6HA* parasites were incubated with 50 μM biotin (Sigma-Aldrich, cat#B4639) at 22 °C for 3 h. After biotinylation, the parasites were pelleted, washed three times with 1 mL ice-cold PBS to remove biotin, and lysed via ultrasonication in buffer A supplemented with protease inhibitor cocktail and PMSF. The lysate was incubated on ice for 10 min and centrifuged at 14,000 g at 4 °C for 10 min. The supernatant was mixed with 50 μL pre-balanced streptavidin sepharose (Thermal Scientific, cat#SA10004) at 4 °C overnight. The beads were washed five times with 1 mL ice-cold buffer A and washed five times with 1 mL ice-cold PBS. The washed beads were resuspended in 200 μL 100 mM TrisHCl pH 8.5 and digested with 1 μg trypsin at 37 °C overnight.

Peptide desalting and mass spectrometry

Trifluoroacetic acid (TFA, Sigma-Aldrich, cat#T6508) was added to the trypsin-digested sample to a final concentration of 1%, and the precipitation of sodium deoxycholate was removed by centrifugation. The resulting supernatant was desalted using in-house-made StageTips that were packed with SDB-RPS (3 M EMPORE, cat#2241) and conditioned with 50 μL of 100% acetonitrile (ACN, Sigma-Aldrich, cat# 34851). After loading the supernatant onto the StageTips, centrifugation was performed at 3000 × *g* for 5 minutes. The StageTips were washed twice with 50 μL of 1% TFA/isopropyl alcohol (Sigma-Aldrich, cat# I9030) followed by a wash with 50 μL of 0.2% TFA. The peptides were eluted in glass vials (CNW Technologies, cat#A3511040) using 80% ACN/5% NH_4OH and dried at 45 °C using a vacuum centrifuge (Eppendorf, cat#5305). The peptide samples were resolved in 2% ACN/0.1FA for LC-MS analysis. Liquid chromatography was performed on a high-pressure nano-flow chromatography system (Elute UHPLC, Bruker Daltonics). Peptides were separated on a reversed-phase column (40 cm × 75 μm i.d.) at 50 °C packed with 1.8 μm 120 Å C18 material (Welch, Shanghai, China) with a pulled emitter tip. A solution is 0.1% FA in H_2O, and B solution is 0.1% FA in ACN. The gradient time was 60 min, and the total run time was 75 min including washes and equilibration. Peptides were separated with a linear gradient from 0 to 5% B within 5 min, followed by an increase to 30% B within 55 min and further to 35% B within 5 minutes, followed by a washing step at 95% B and re-equilibration. LC was coupled online to a hybrid TIMS quadrupole time-of-flight mass spectrometer (Bruker timsTOF Pro) via a CaptiveSpray nano-electrospray ion source. We performed data-dependent data acquisition in PASEF mode with 10 PASEF scans per topN acquisition cycle. Singly charged precursors were excluded by their position in the m/z-ion mobility plane and precursors that reached a 'target value' of 20,000 a.u. were dynamically excluded for 0.4 minutes. We used 100 milliseconds to accumulate and elute ions in the TIMS tunnel. The MS1 m/z-range was acquired from 100 to 1700, and the ion mobility range from 1.5 to 0.7 V cm^{-2}. For data-independent acquisition, we adopted the isolation scheme of 25 Da × 32 windows to cover 400–1200 mz. DIA files (raw) files were input to DIA-NN (v1.8.1)[65] FASTA files downloaded from https://www.uniprot.org (UP000072874)[66] were added. "FASTA digest for library-free search" and "Deep learning-based spectra, RTs, and IMs prediction" were enabled. "Generate spectral library" was also enabled. "Protein inference" was set to "gene". Other parameters were kept at the default settings. Statistical analysis by Perseus software (version 1.6.10.43) were performed as previously reported[67]. Parasite protein intensities were imported into Perseus. Protein abundances were normalized with total intensities of all proteins per run and then log2 transformed. The Pearson correlation analysis, hierarchical clustering, and volcano plots were performed with default settings.

Proximity ligation assay (PLA)

PLA assay was performed to detect in situ protein interaction using a commercial kit (Sigma-Aldrich, cat#DUO92008, DUO92001, DUO92005, and DUO82049). Ookinetes were fixed with 4% paraformaldehyde for 30 minutes, permeabilized with 0.1% Triton X-100 for 10 minutes at room temperature, and blocked with a blocking solution overnight at 4 °C. The primary antibodies were diluted in the Duolink Antibody Diluent and incubated with ookinetes in a humidity chamber overnight at 4 °C. After removing the primary antibodies, the ookinetes were rinsed twice with wash buffer A. The PLUS and MINUS PLA probes were diluted in Duolink Antibody Diluent, and ookinetes were incubated in a humidity chamber for 1 h at 37 °C. Next, ookinetes were rinsed twice with wash buffer A and incubated with the ligation solution for 30 min at 37 °C. Ookinetes were rinsed twice with wash buffer A and incubated with the amplification solution for 100 min at 37 °C in the dark. After rinsing twice with 1 × wash buffer B and one time with 0.01 × wash buffer B, ookinetes were stained with Hoechst 33342 and washed twice with PBS. Images were captured and processed in a Zeiss LSM 880 confocal microscope using identical settings.

Scanning electron microscopy

Purified ookinetes were fixed with 2.5% glutaraldehyde in 0.1 M phosphate buffer at 4 °C overnight, rinsed three times with PBS, and fixed with 1% osmium tetroxide for 2 h. Fixed cells were dehydrated using a graded acetone series, CO_2-dried in a critical-point drying device, and gold-coated in a sputter coater as previously[68]. The samples were imaged using a SUPRA55 SAPPHIRE Field Emission Scanning Electron Microscope.

Episomal expression of protein

The genes encoding the NAD^+ probe mCherry-FiNad or mCherry-cpYFP were driven by the 5'-UTR (1998 bp) of the *hsp86* gene and the 3'-UTR (803 bp) of the *dhfr* gene. The expressing cassette was inserted into the pL0019-derived vector with human *dhfr* for pyrimethamine selection[19]. Purified schizonts were electroporated with 10 μg plasmid DNA. Transfected parasites were immediately intravenously injected into a naïve mouse and exposed to pyrimethamine (70 μg/mL) for 5–8 days. After pyrimethamine selection, 4.0×10^6 parasitized erythrocytes were injected intravenously into phenylhydrazine-pretreated naïve mice to induce gametocytes and were kept under pyrimethamine pressure. Mice with high gametocytaemia were used for further study.

Measurement of intracellular NAD^+

To measure the intracellular NAD^+ level in the ookinete development of *Plasmodium*, we used a genetically encoded NAD^+ fluorescent biosensor FiNad[41]. Parasite gametocytes expressing the mCherry-FiNad or mCherry-cpYFP sensor proteins were cultured at 22 °C for in vitro ookinete development. Different stages of parasites from the cultures were harvested at 0, 0.5, 4, 8, 12, and 16 h. The harvested parasites were collected in 200 μL PBS, washed twice with PBS, and stained with Hoechst 33342 at room temperature for 10 minutes. After centrifuging at 500 g for 3 min, the parasite pellets were re-suspended in 100 μL of 3% low melting agarose (Sigma-Aldrich, cat#A9414), and transferred evenly on the bottom of a 35 mm culture dish. Parasites were placed at room temperature for 15 min and imaged using a Zeiss LSM 880 confocal microscope. Raw data were exported to ImageJ software as 12 bit TIF for analysis. The pixel-by-pixel ratio of the 488 nm excitation image to the 555 nm excitation image in a cell was used to pseudocolor the images in HSB color space. The RGB value (255, 0, 255) represents the lowest ratio, the red (255, 0, 0) represents the highest ratio, and the color brightness is proportional to the fluorescent signals in both channels.

Bioinformatic searches and tools

The genomic sequences of target genes were downloaded from the PlasmoDB database (http://plasmodb.org/plasmo/app/)[69]. The sgRNA of target genes was searched using the database EuPaGDT (http://grna.ctegd.uga.edu/)[70]. The amino acid sequences of protein homologs were downloaded from UniProt (https://www.uniprot.org/). The alignment of protein sequences was analyzed with MUSCLE (Version 5.1), and aligned sequences were trimmed with TrimAl (Version 1.4.1). The acetylation residues in protein were predicted using CSS-Palm 4.0 (http://csspalm.biocuckoo.org/)[36].

Quantification and statistical analysis

For quantifying protein polarization at OES in ookinetes, the fluorescent signals of protein were acquired using identical parameters in the microscope and analyzed by using Fiji software[71]. 30 cells were randomly chosen in each group. For quantifying the ookinete gliding speed, images were quantified using Fiji software. Statistical analysis was performed using GraphPad Prism 8.0. Details of statistical methods are described in the figure legends.

Reporting summary

Further information on research design is available in the Nature Portfolio Reporting Summary linked to this article.

Data availability

All relevant data in this study are submitted as supplementary source files. Source data are provided in this paper. The mass spectrometry proteomic data have been deposited in the ProteomeXchange with identifier PXD056305 (https://www.iprox.cn/page/project.html?id=IPX0009818000). Source data are provided with this paper.

References

1. WHO. World malaria report *2023*. (WHO, 2023).
2. Bennink, S., Kiesow, M. J. & Pradel, G. The development of malaria parasites in the mosquito midgut. *Cell. Microbiol.* **18**, 905–918 (2016).
3. Guttery, D. S. et al. Commit and transmit: Molecular players in sexual development and zygote differentiation. *Trends Parasitol.* **31**, 676–685 (2015).
4. Josling, G. A. & Llinás, M. Sexual development in parasites: knowing when it's time to commit. *Nat. Rev. Microbiol.* **13**, 573–587 (2015).
5. Aly, A. S. I., Vaughan, A. M. & Kappe, S. H. I. Malaria parasite development in the mosquito and infection of the mammalian Host. *Annu. Rev. Microbiol.* **63**, 195–221 (2009).
6. Al-Khattaf, F. S., Tremp, A. Z. & Dessens, J. T. Plasmodium alveolins possess distinct but structurally and functionally related multi-repeat domains. *Parasitol. Res.* **114**, 631–639 (2015).
7. Keeley, A. & Soldati, D. The glideosome: a molecular machine powering motility and host-cell invasion by Apicomplexa. *Trends Cell Biol.* **14**, 528–532 (2004).
8. Dessens, J. T. et al. CTRP is essential for mosquito infection by malaria ookinetes. *EMBO J.* **18**, 6221–6227 (1999).
9. Boucher, L. E. & Bosch, J. The apicomplexan glideosome and adhesins - Structures and function. *J. Struct. Biol.* **190**, 93–114 (2015).
10. Hirai, M. et al. PbGCβ is essential for Ookinete motility to invade midgut cell and for successful completion of parasite life cycle in mosquitoes. *J. Biochem.* **140**, 747–757 (2006).
11. Brochet, M. et al. Phosphoinositide metabolism links cGMP-dependent protein jinase G to essential Ca^{2+} signals at key decision points in the life cycle of malaria parasites. *Plos Biol.* **12**, https://doi.org/10.1371/journal.pbio.1001806 (2014).
12. Moon, R. W. et al. A cyclic GMP signalling module that regulates gliding motility in a malaria parasite. *PLoS Pathog.* **5**, e1000599 (2009).
13. Ishino, T. et al. A calcium-dependent protein kinase regulates Plasmodium ookinete access to the midgut epithelial cell. *Mol. Microbiol.* **59**, 1175–1184 (2006).
14. Baker, D. A. Cyclic nucleotide signalling in malaria parasites. *Cell. Microbiol.***13**, 331–339 (2011).
15. Baker, D. A. Adenylyl and guanylyl cyclases from the malaria parasite. *Iubmb Life* **56**, 535–540 (2004).
16. Linder, J. U. & Schultz, J. E. Guanylyl cyclases in unicellular organisms. *Mol. Cell. Biochem.* **230**, 149–158 (2002).
17. Baker, D. A. et al. Cyclic nucleotide signalling in malaria parasites. *Open Biol.* **7**, https://doi.org/10.1098/rsob.170213 (2017).
18. Linder, J. U. et al. Guanylyl cyclases with the topology of mammalian adenylyl cyclases and an N-terminal P-type ATPase-like domain in Paramecium, Tetrahymena and Plasmodium. *Embo J.* **18**, 4222–4232 (1999). p.
19. Gao, H. et al. ISP1-Anchored polarization of GCbeta/CDC50A complex initiates Malaria Ookinete Gliding Motility. *Curr. Biol.* **28**, 2763–2776(2018).
20. Günay-Esiyok, Ö. & Gupta, N. Chimeras of P4-ATPhase and guanylate cyclase in pathogenic protists. *Trends Parasitol.* **36**, 382–392 (2020).
21. Brochet, M. cGMP Signalling: Malarial guanylyl cyclase leads the way. *Curr. Biology* **28**, R939–R941 (2018).
22. Billker, O. CRISPRing the elephant in the room. *Cell Host Microbe* **24**, 754–755 (2018).
23. Capone, V. et al. HAT1: Landscape of biological function and role in cancer. *Cells* **12**, 1075 (2023).
24. Narita, T., Weinert, B. T. & Choudhary, C. Functions and mechanisms of non-histone protein acetylation. *Nat. Rev. Mol. Cell Biol.* **20**, 156–174 (2019).
25. Wu, F. et al. Acetylation-dependent coupling between G6PD activity and apoptotic signaling. *Nat. Commun.* **14**, 6208 (2023).
26. Schwer, B. & Verdin, E. Conserved metabolic regulatory functions of sirtuins. *Cell Metab.* **7**, 104–112 (2008). p.
27. Wang, F. et al. SIRT5 Desuccinylates and activates pyruvate kinase M2 to block macrophage IL-1β production and to prevent DSS-induced colitis in mice. *Cell Rep.* **19**, 2331–2344 (2017).
28. Tissenbaum, H. A. & Guarente, L. Increased dosage of a sir-2 gene extends lifespan in Caenorhabditis elegans. *Nature* **410**, 227–230 (2001).
29. Tonkin, C. J. et al. Sir2 paralogues cooperate to regulate virulence genes and antigenic variation in Plasmodium falciparum. *Plos Biol.*771–788 (2009). .
30. Freitas-Junior, L. H. et al. Telomeric heterochromatin propagation and histone acetylation control mutually exclusive expression of antigenic variation genes in malaria parasites. *Cell* **121**, 25–36 (2005).
31. Duraisingh, M. T. et al. Heterochromatin silencing and locus repositioning linked to regulation of virulence genes in Plasmodium falciparum. *Cell* **121**, 13–24 (2005).
32. Zhang, C. et al. Efficient editing of malaria parasite genome using the CRISPR/Cas9 system. *mBio* **5**, e01414 (2014).
33. Zhang, C. et al. CRISPR/Cas9 mediated sequential editing of genes critical for ookinete motility in Plasmodium yoelii. *Mol. Biochem. Parasitol.* **212**, 1–8 (2017).
34. Söderberg, O. et al. Direct observation of individual endogenous protein complexes by proximity ligation. *Nat. Methods* **3**, 995–1000 (2006).
35. Frénal, K. et al. Gliding motility powers invasion and egress in Apicomplexa. *Nat. Rev. Microbiol.* **15**, 645–660 (2017).
36. Li, A. et al. Prediction of N-acetylation on internal lysines implemented in Bayesian Discriminant Method. *Biochem. Biophys. Res. Commun.***350**, 818–824 (2006).
37. Min, J. R. et al. Crystal structure of a SIR2 homolog-NAD complex. *Cell* **105**, 269–279 (2001).

38. Imperatore, F. et al. SIRT1 regulates macrophage self-renewal. *Embo J.* **36**, 2353–2372 (2017).
39. Yang, Z. K. et al. A malaria parasite phospholipid flippase safeguards midgut traversal of ookinetes for mosquito transmission. *Sci. Adv.* **7**, eabf6015 (2021).
40. Imai, S. & Guarente, L. NAD^+ and sirtuins in aging and disease. *Trends Cell Biol.* **24**, 464–471 (2014).
41. Zou, Y. J. et al. Illuminating NAD^+ metabolism in live cells and using a genetically encoded fluorescent sensor. *Dev. Cell* **53**, 240 (2020).
42. O'Hara, J. K. et al. Targeting NAD^+ metabolism in the human malaria parasite Plasmodium falciparum. *PLoS ONE* **9**, e94061 (2014).
43. Donu, D., Sharma, C. A.-O. & Cen, Y. Plasmodium falciparum nicotinamidase as a novel Antimalarial Target. *Biomolecules* **12**, 1109 (2022).
44. Cunningham, D. A. et al. Host immunity modulates transcriptional changes in a multigene family (yir) of rodent malaria. *Mol. Microbiol.* **58**, 636–647 (2005).
45. Ukegbu, C. V. et al. Identification of genes required for Plasmodium gametocyte-to-sporozoite development in the mosquito vector. *Cell Host Microbe* **31**, 1539–1551 (2023).
46. Kanyal, A. et al. PfHDAC1 is an essential regulator of asexual proliferation and host cell invasion genes with a dynamic genomic occupancy responsive to artemisinin stress. *mBio* **15**, https://doi.org/10.1128/mbio.02377-23 (2024).
47. Nyonda, M. A. et al. N-acetylation of secreted proteins in Apicomplexa is widespread and is independent of the ER acetyl-CoA transporter AT1. *J. Cell Sci.* **135**, jcs259811 (2022).
48. Sen, U. et al. Inhibition of PfMYST histone acetyltransferase activity blocks growth and survival. *Antimicrob. Agents Chemother.* **65**, e00953–20 (2021).
49. Trenholme, K. et al. Lysine acetylation in sexual stage malaria parasites is a target for antimalarial small molecules. *Antimicrob. Agents Chemother.* **58**, 3666–3678 (2014).
50. Miao, J. et al. The MYST family histone acetyltransferase regulates gene expression and cell cycle in malaria parasite. *Mol. Microbiol.* **78**, 883–902 (2010).
51. Li, Z. K. et al. Plasmodium transcription repressor AP2-O3 regulates sex-specific identity of gene expression in female gametocytes. *Embo Rep.* **22**, e51660 (2021).
52. Yeoh, L. M. et al. Comparative transcriptomics of female and male gametocytes in Plasmodium berghei and the evolution of sex in alveolates. *BMC Genomics* **18**, 734 (2017).
53. Ji, X. et al. NAD^+-Consuming enzymes in stem cell homeostasis. *Oxid. Med. Cell. Longev.* **2023**, 1–11 (2023).
54. Sahar, S. et al. Altered behavioral and metabolic circadian rhythms in mice with disrupted NAD^+ oscillation. *Aging* **3**, 794–802 (2011).
55. Navas, L. E. & Carnero, A. NAD^+ metabolism, stemness, the immune response, and cancer. *Signal Transduction Target.Ther.* **6**, 2 (2021).
56. Covarrubias, A. J. et al. NAD^+ metabolism and its roles in cellular processes during ageing. *Nat. Rev. Mol. Cell Biol.* **22**, 119–141 (2021).
57. Cantó, C. et al. AMPK regulates energy expenditure by modulating NAD^+ metabolism and SIRT1 activity. *Nature* **458**, 1056–1060 (2009).
58. Gerhart-Hines, Z. et al. Metabolic control of muscle mitochondrial function and fatty acid oxidation through SIRT1/PGC-1α. *EMBO J.* **26**, 1913–1923 (2007).
59. Pirinen, E. et al. Niacin cures systemic NAD^+ deficiency and improves muscle performance in adult-onset mitochondrial myopathy. *Cell Metab.* **31**, 1078–1090.(2020).
60. Cantó, C. et al. The NAD^+ Precursor nicotinamide riboside enhances oxidative metabolism and protects against high-fat diet-induced obesity. *Cell Metab.* **15**, 838–847 (2012).
61. Zhang, C. et al. Efficient editing of malaria parasite genome using the CRISPR/Cas9 system. *mBio* **5**, e01414–14 (2014).
62. Jiang, Y. et al. An intracellular membrane protein GEP1 regulates xanthurenic acid induced gametogenesis of malaria parasites. *Nat. Commun.* **11**, 1764 (2020).
63. Carter, V. et al. Isolation of Plasmodium berghei ookinetes in culture using Nycodenz density gradient columns and magnetic isolation. *Malar. J.* **2**, 35 (2003).
64. Meijering, E., Dzyubachyk, O. & Smal. I. Methods for cell and particle tracking. *Methods Enzymol.* 183–200 https://doi.org/10.1016/b978-0-12-391857-4.00009-4 (2012).
65. Demichev, V. et al. DIA-NN: neural networks and interference correction enable deep proteome coverage in high throughput. *Nat. Methods* **17**, 41–44 (2019).
66. Guan, J. et al. An axonemal intron splicing program sustains Plasmodium male development. *Nat. Commun.* **15**, 4697 (2024).
67. Tyanova, S. et al. The Perseus computational platform for comprehensive analysis of (prote)omics data. *Nat. Methods* **13**, 731–740 (2016).
68. Orfano, A. S. et al. Species-specific escape of Plasmodium sporozoites from oocysts of avian, rodent, and human malarial parasites. *Malar. J.* **15**, https://doi.org/10.1186/s12936-016-1451-y (2016).
69. Aurrecoechea1, C. et al. PlasmoDB: a functional genomic database for malaria parasites. *Nucleic Acids Res.* https://doi.org/10.1093/nar/gkn814 (2009).
70. Peng, D. & Tarleton, R. EuPaGDT: a web tool tailored to design CRISPR guide RNAs for eukaryotic pathogens. *Microb. Genom.* **1**, https://doi.org/10.1099/mgen.0.000033 (2015).
71. Schindelin, J. et al. Fiji: an open-source platform for biological-image analysis. *Nat. Methods* **9**, 676–682 (2012).

Acknowledgements

This work was supported by the National Natural Science Foundation of China (32170427 by J.Y. and 32270503 by H.C.), the National Key Research and Development Program of China (2024YFC2309700), the 111 Project sponsored by the State Bureau of Foreign Experts and Ministry of Education of China (BP0618017 by J.Y.), and the Xiamen University Double First Class Construction Project (Biology, DFC2024001 by J.Y.).

Author contributions

Y.S. and J.Y. designed the project. Y.S., L.W., and M.J. generated the modified parasites. Y.S., L.W., and M.J. performed phenotype analysis, protein analysis, imaging analysis, and electron microscopy analysis. Y.S. performed the bioinformatics analysis. C.Z. performed, analyzed, and supervised the protein mass spectrometry. Y.S. and J.Y. supervised the work. Y.S., H.C., and J.Y. wrote the manuscript.

Competing interests

The authors declare no competing interests.

Additional information

Supplementary information The online version contains supplementary material available at https://doi.org/10.1038/s41467-025-57517-y.

Correspondence and requests for materials should be addressed to Chuan-qi Zhong, Huiting Cui or Jing Yuan.

Peer review information *Nature Communications* thanks Rita Tewari who co reviewed with Mohammad Zeeshan, Ryuji YanaseCatherine Merrick and the other, anonymous, reviewer(s) for their contribution to the peer review of this work. A peer review file is available.